

# DBC1 is a key positive regulator of enhancer epigenomic writers KMT2D and p300

Hwa Jin Kim<sup>1,2</sup>, Sue Jin Moon<sup>1,2</sup>, Sanghoon Hong<sup>3</sup>, Hong-Hee Won<sup>2,3</sup> and Jeong Hoon Kim<sup>1,2,\*</sup>

<sup>1</sup>Department of Health Sciences and Technology, Samsung Advanced Institute for Health Sciences and Technology, Sungkyunkwan University, Seoul, 06351, South Korea, <sup>2</sup>Research Institute for Future Medicine, Samsung Medical Center, Seoul, 06351, South Korea and <sup>3</sup>Department of Digital Health, Samsung Advanced Institute for Health Sciences and Technology, Sungkyunkwan University, Seoul, 06351, South Korea

Received May 12, 2022; Revised June 14, 2022; Editorial Decision June 20, 2022; Accepted June 24, 2022

## ABSTRACT

Histone modification is a key epigenetic mechanism for regulation of chromatin dynamics and gene expression. Deleted in breast cancer 1 (DBC1) has been shown to act as a negative regulator of epigenetic modifiers and as a co-activator for nuclear receptors and other transcription factors. However, little is known about the role of DBC1 in the regulation of histone modifications and chromatin landscapes. Here, we analyzed genome-wide profiles of active enhancer and promoter marks in colorectal cancer cells and report DBC1 as a critical positive regulator of histone epigenetic writers KMT2D (H3K4 methyltransferase) and p300 (histone acetyltransferase). DBC1 is required for establishing the landscape of active enhancers, for genome-wide chromatin binding and enhancer recruitment of KMT2D and p300, and for gene activation involved in colorectal cancer progression. DBC1 interacts directly with KMT2D and p300, and enhances KMT2D-mediated histone H3K4 methylation (H3K4me1/2/3) and p300-mediated H3 acetylation. Importantly, DBC1 contributes to super-enhancer formation and function by facilitating the recruitment of KMT2D and p300 and by enhancing their functional interaction and cooperative crosstalk. Our results highlight the critical role of DBC1 as a key positive regulator of KMT2D and p300, and provide insights into regulatory mechanisms underlying the interplay between the enhancer epigenomic writers in enhancer activation.

## INTRODUCTION

Histone modifications play fundamental roles in the epigenetic regulation of gene expression and chromatin dy-

namics (1). Recent epigenomic analyses of histone modifications have provided insights into the chromatin signatures of active enhancers (AEs) and active promoters (APs) in mammalian genomes. While APs are enriched for tri-methylated H3K4 (H3K4me3) and acetylated H3K9 and H3K14 (H3K9/K14ac), AEs can be identified by mono-methylated H3K4 (H3K4me1) and acetylated H3K27 (H3K27ac) (1–3). In addition, enhancers can be classified into typical enhancers and super-enhancers (SEs) (4,5). SEs are large clusters of AEs densely occupied by transcription factors (TFs), co-activators and AE marks such as H3K27ac, and drive expression of genes that play critical roles in regulating normal and pathological cell physiology (6,7). The development and progression of cancer are driven not only by genetic alterations but also by epigenetic dysregulation of gene expression (1,8,9). Accumulating evidence has shown that cancer cells frequently acquire cancer-specific SEs to drive high levels of oncogene expression and resistance to chemotherapy (4–8). For example, a large fraction of SEs acquired by colorectal cancer (CRC) cells are associated with oncogenes, and the acquired SEs are enriched in binding motifs for TCF4/TCF7L2, the terminal TF of the oncogenic Wnt/ $\beta$ -catenin signaling pathway in CRC cells (8,10).

Previous biochemical and chromatin immunoprecipitation (ChIP) sequencing (ChIP-seq) studies have shown that the histone methyltransferase (HMT) KMT2D/MLL4 and the histone acetyltransferase (HAT) p300 are the key epigenetic writers for AE signatures (11–14). KMT2D exists in multiprotein complexes containing a set of core components, ASH2L, RBBP5, WDR5 and DPY30, shared by other members of the KMT2 family. As a major H3K4me1/2 HMT, KMT2D is enriched in AEs including SEs marked by high levels of H3K27ac and required for p300 binding and p300-mediated H3K27ac deposition at AEs (12–14). Although previous studies have reported cooperative functional interaction of KMT2D and p300 in enhancer-associated histone modifications and enhancer

\*To whom correspondence should be addressed. Tel: +82 2 3410 0532; Fax: +82 2 3410 0534; Email: jeongkim@skku.edu

activation (12–15), the key regulators and underlying regulatory mechanisms for the cooperativity of KMT2D and p300 remain unclear.

Deleted in breast cancer 1 (DBC1; also known as CCAR2) has been identified as a co-activator of several TFs, including p53, estrogen receptor  $\alpha$  (ER $\alpha$ ), androgen receptor (AR), AR-V7, PEA3, TCF4/LEF1- $\beta$ -catenin and PROX1, and as a negative regulator of epigenetic modifiers such as the deacetylases SIRT1 and HDAC3, HMT SUV39H1 and ubiquitin E3 ligases MDM2 and CHIP (16–26). For example, we have shown that DBC1 acts as a co-activator for ER $\alpha$  and PEA3 in breast cancer cells and for AR and AR-V7 in prostate cancer cells (17,19,20). Mechanistically, DBC1 binds to and inhibits SIRT1-mediated deacetylation of ER $\alpha$  and PEA3, and suppresses CHIP-mediated AR and AR-V7 ubiquitination and degradation, thereby enhancing their transcriptional activities and recruitment to target enhancers and promoting cancer progression. In addition, we have shown that DBC1 also functions as a co-activator of  $\beta$ -catenin, by protecting  $\beta$ -catenin from SIRT1-mediated deacetylation, as well as Wnt/ $\beta$ -catenin-inducible TFs PROX1 and MACC1, suggesting DBC1 as a critical regulator in Wnt/ $\beta$ -catenin-PROX1-MACC1 signaling-driven CRC progression (21,22). However, despite increasing knowledge on the role of DBC1 as a regulator of epigenetic modifiers, little is known about whether DBC1 can impact histone modifications and chromatin dynamics through regulating the activity of epigenetic modifiers. In this study, we report that DBC1 functions as a key regulator of enhancer epigenomic writers, KMT2D and p300, and of the cross-talk between KMT2D-mediated H3K4 methylation and p300-mediated H3 acetylation in CRC cells.

## MATERIALS AND METHODS

### Cell culture and transient transfection

SW480 wild type (WT), SW480 DBC1 knock-out (D1KO) and 293T cells were maintained in Dulbecco's modified Eagle's medium (DMEM) supplemented with 10% fetal bovine serum (FBS). SW480 D1KO cells were described previously (21). HCT116 WT and HCT116 D1KO cells were cultured in RPMI 1640 media supplemented with 10% FBS. All cell lines were purchased from the American Type Culture Collection (ATCC), routinely tested for mycoplasma contamination by PCR, and authenticated by short tandem repeat profiling. For transient transfection, cells were transfected with expression vectors using jetPEI (Polyplus).

### Plasmids

The following plasmids were described previously: pSG5.HA-DBC1, pGEX-4T-1-DBC1, HA-p300 (17); p3 $\times$ FLAG.CMV10-DBC1 (19); pCI.FLAG-p300, pGEX-p300-NTD, pGEX-p300-KIX, pGEX-p300-CH3, pGEX-p300-Q (27); and pHR.CMV.puro.Sin8-shNS, pLKO.1-sh $\beta$ -catenin#3, pAcKRS-3, pCDF PylT-1 (20,21). cDNAs encoding histone H3.1 from GST-hH3 (a kind gift from Woojin An, University of Southern California), H3.3 from pCMV-SPORT6-hH3.3 (Open Biosystems,

#MHS6278-202759238), full-length human KMT2D from pCMV-HA-KMT2D (a kind gift from Laura Pasqualucci, Columbia University) and TurboID from FLAG-TurboID (Addgene #124646) were cloned into p3 $\times$ FLAG.CMV10 (Sigma-Aldrich). H3K27R and H3K4R mutants were generated with the QuikChange site-directed mutagenesis kit (Agilent Technologies). cDNA encoding hH3 was cloned into pCDF PylT-1. pCDF PylT-1-H3 constructs carrying an amber mutation at K4, K9 or K27 were generated with the QuikChange site-directed mutagenesis kit. PCR-amplified cDNA fragments of KMT2D, p300 and DBC1 were cloned into the indicated vectors (with amino acid numbers): pSG5.HA-KMT2D [1–420, 366–939, 933–1248, 1201–1838, 1837–2229, 2214–2690, 2582–3216, 3216–3689, 3690–4008, 4000–4512, 4506–5040, 5011–5537, 5175–5537 or 5326–5537 (SET)]; pGEX-4T-1-KMT2D 5326–5537 (SET); p3 $\times$ FLAG.CMV10-KMT2D 5326–5537 (SET); p3 $\times$ FLAG.CMV10-TurboID-KMT2D 5326–5537 (SET); pSG5.HA-p300 1048–1673 (Br-HAT); pGEX-4T-1-p300 [1048–1673 (Br-HAT), 1048–1290 (Br-PHD) or 1195–1673 (HAT)]; pSG5.HA-DBC1 [1–270 (NTD), 271–680 (M), 271–923 ( $\Delta$ N) or 1–680 ( $\Delta$ C)]; and pGEX-4T-1-DBC1 (NTD or  $\Delta$ N). PCR-amplified CBP 1095–1711 (Br-HAT) from pcDNA3b.FLAG.CBP.HA (Addgene #32908) was cloned into pGEX-4T-1. pLKO.1-shKMT2D-puro, a lentiviral vector expressing short hairpin RNAs (shRNAs) against KMT2D, was purchased from Sigma-Aldrich (TRCN0000013139). The LEF1 shRNA expression lentiviral vector (pLKO.1-shLEF1) was generated by inserting shRNA oligonucleotides (Supplementary Table S3) into pLKO.1 (Sigma-Aldrich). LentiCRISPRv2.1-dCas9 vector was constructed by inserting a synthetic sequence containing multiple cloning sites (BamHI-HpaI-AscI-XhoI-BglII) into the BamHI site of LentiCRISPRv2-dCas9 (Addgene, #112233). To generate a lentiviral vector expressing dCas9-DBC1 fusion protein and a single guide RNA (sgRNA) targeting the PROX1 SE (LentiCRISPRv2.1-dCas9-DBC1-sgPROX1#1.SE), sgRNA#1 oligonucleotides and PCR-amplified DBC1 cDNA were cloned into BsmBI and HpaI-XhoI sites of LentiCRISPRv2.1-dCas9, respectively. To create an sgRNA expression vector (pU6-sgRNA), pSpCas9(BB)-2A-GFP (PX458) (Addgene, #48138) was digested with KpnI/EcoRI to remove the Cas9-green fluorescent protein (GFP) cassette, filled-in and blunt-end ligated. Two individual sgRNA oligonucleotides (sgPROX1#4 and #5) targeting the PROX1 SE were cloned into the BbsI site of pSpU6-sgRNA. sgRNA sequences used are indicated in Supplementary Table S3. For lentiviral infection, lentiviral particles were produced as previously described (28).

### Antibodies, peptides and site-specifically acetylated H3 proteins

The following antibodies were used in this study: anti-H3K4me3, 39159 (Active Motif); anti-H3K4me1, ab8895 (Abcam); anti-H3K27ac, ab4729 (Abcam); anti-H3K9/K14ac, SC-8655R (Santa Cruz Biotechnology); anti-H3K4ac, 39381 (Active Motif) and 07-539 (Millipore); anti-H3K9ac, 07-352 (Millipore); anti-H3K18ac, A7257 (ABclonal); anti-H3K4me2, 07-030 (Millipore); anti-

H3K27me2/me3, 39535 (Active Motif); anti-H3, ab1791 (Abcam); anti-GST, B-14 (Santa Cruz Biotechnology); anti-DBC1, A300-434A (Bethyl Laboratories) and A7126 (ABclonal); anti-KMT2D/MLL4, HPA035977 (Atlas Antibodies) and ABE1867 (Millipore); anti-p300, A300-358A (Bethyl Laboratories) and C-20 (Santa Cruz Biotechnology); anti-ASH2L, A4892 (ABclonal); anti-RBBP5, A6965 (ABclonal); anti-WDR5, A3259 (ABclonal); anti-UTX, A302-374A (Bethyl Laboratories); anti-LEF1, GTX129186 (GeneTex); anti-PROX1, 07-537 (Millipore); anti- $\beta$ -catenin, E-5 (Santa Cruz Biotechnology) and 160154 (BD Biosciences); anti-acetylated lysine, 9441 (Cell signaling Technology); anti-HA, 3F10 (Roche); anti-HA-agarose, A2095 (Sigma-Aldrich); anti-FLAG, M2 (Sigma-Aldrich); anti-FLAG M2-agarose (Sigma-Aldrich); anti-S-Tag A190-135A (Bethyl Laboratories); anti-GAPDH, LFP-A0018 (AbFrontier); streptavidin-HRP, 21130 (Thermo Scientific). The following biotin-conjugated synthetic peptides were used for the antibody specificity test: unmodified H3 (1–21), 12-403 (Millipore); H3K9/K14ac (1–21), 12-402 (Millipore); H3K4ac (1–21), AS-65207 (AnaSpec); H3K4me3 (1–21), AS-64357 (AnaSpec); H3K27ac (15–34), 12-0042 (EpiCypher). Site-specifically acetylated H3 proteins (H3K4ac, H3K27ac and H3K9ac) were generated and purified by a strategy described previously (20,21).

### CRISPR/Cas9-mediated knockout of DBC1

pRGEN-Cas9-CMV, three guide RNA expression plasmids (pRGEN-human-DBC1-U6-SG #1, #2 and #3) targeting exon 3 of the DBC1 gene and a surrogate reporter pRGS2 were purchased from ToolGen and transfected into HCT116 and 293T cells. Transfected cells were sorted using a FACS Aria III (BD Biosciences), and single clones were isolated by limiting dilution and expansion. Clones were screened for DBC1 expression by immunoblot and subsequently validated by DNA sequencing of PCR products spanning exon 3 of the DBC1 gene.

### ChIP and ChIP-seq

ChIP assays were performed as described previously with some modifications (21,28). For modified histone ChIP assays, SW480 cells were fixed with 1% formaldehyde for 10 min and quenched by 0.125 M glycine for 5 min. Cross-linked cells were washed twice with cold phosphate-buffered saline (PBS) and incubated with buffers containing complete EDTA-free protease inhibitor cocktail (Roche): hypotonic buffer (10 mM HEPES-KOH, pH 7.8, 10 mM KCl, 1.5 mM MgCl<sub>2</sub>) for 20 min and nuclear lysis buffer (50 mM Tris-HCl, pH 8.0, 10 mM EDTA, 1% SDS) for 10 min. Chromatin fractions were sonicated using a Bioruptor (Cosmobio) for 15 min (30 s on/30 s off, high power) to generate DNA fragments of ~100–300 bp. Sheared chromatin was diluted 10-fold with ChIP dilution buffer (20 mM Tris-HCl, pH 8.0, 167 mM NaCl, 1.2 mM EDTA, 0.01% SDS, 1.1% Triton X-100), incubated with 1–5  $\mu$ g of the indicated antibodies and recovered with Protein A/G Plus-Agarose (Santa Cruz Biotechnology). After washing with TSE I (20 mM Tris-HCl, pH 8.0, 150 mM NaCl,

2 mM EDTA, 0.1% SDS, 1% Triton X-100), TSE II (20 mM Tris-HCl, pH 8.0, 500 mM NaCl, 2 mM EDTA, 0.1% SDS, 1% Triton X-100), TSE III (10 mM Tris-HCl, pH 8.0, 0.25 M LiCl, 1 mM EDTA, 1% deoxycholate, 1% NP-40) and TE buffers, bound ChIP complexes were eluted with ChIP elution buffer (0.1 M NaHCO<sub>3</sub>, 1% SDS), reverse cross-linked by incubation with RNase A and 0.3 M NaCl at 65°C overnight, and treated with proteinase K at 45°C for 1 h. ChIP DNAs were purified using a PCR Purification Kit (Qiagen), and eluted DNAs were used for conventional ChIP-qPCR or ChIP-seq library preparation. A SimpleChIP Enzymatic Chromatin IP kit (Cell signaling Technology) was used for ChIP of KMT2D, p300, DBC1, LEF1 and  $\beta$ -catenin. ChIP-qPCR was performed in triplicate using TB Green Fast qPCR mix (Takara) and the 7900HT FAST Real-Time PCR system (Applied Biosystems). ChIP signals were normalized with inputs, and data were shown as fold change (FC) relative to control IgG signal. ChIP-seq libraries were prepared using the TruSeq ChIP Library Preparation Kit (Illumina) and subjected to next-generation sequencing on a HiSeq 2500 or NovaSeq 6000 (Illumina) to yield 70–100 million 101 bp paired-end reads per sample. The primers used in ChIP-qPCR are listed in Supplementary Table S4.

### ChIP-seq data analysis and identification of SEs

ChIP-seq reads were processed to filter out reads with low quality using Trimmomatic v0.38 and then aligned to the human reference genome (assembly hg19) using Bowtie v1.1.2. Duplicate reads were removed using Picard v1.88. ChIP peaks were called using MACS2 v2.1.1.20160309 with sequences from chromatin extracts of SW480 WT or D1KO as background input control. Peaks yielded with MACS2 [fold enrichment > 4 and false discovery rate (FDR) < 0.01, histone modifications in SW480; FDR < 0.05, HCT116; FDR < 0.05, KMT2D and p300; FDR < 0.0001 and scale-to-large option, DBC1] were selected for further analysis. ChIP-seq tracks were visualized using Bigwig files of ChIP-seq data and the Integrative Genomic Viewer (<http://www.broadinstitute.org/igv/>). Differential peaks were analyzed using merged peaks with the cut-off of  $P < 0.05$  and FC > 1.5. MANorm was used for quantitative comparison of ChIP-seq peaks. Heatmaps of aligned reads, and average signal plots were generated using deepTools v3.3.2 on the Galaxy server (<https://usegalaxy.eu/>) (29). Pearson correlation between ChIP-seq profiles of different histone modifications was calculated using deepTools. Genes associated with ChIP-seq peaks were annotated using ChIPseeker v1.28.3. Pathway enrichment analysis of annotated genes was performed via Metascape (<https://metascape.org/gp/index.html>). ChIPpeakAnno v3.26 was used to determine peak overlaps. Motif enrichment analysis was performed using MEME-ChIP (MEME suite v5.30). SEs were identified using the Rank Ordering of SE (ROSE) algorithm with default parameters using H3K27ac or H3K4ac ChIP-seq signal-based ranking (7). The TCF4/TCF7L2 ChIP-seq datasets (wgEncodeEH002022, wgEncodeEH000629A and wgEncodeEH002071) were downloaded from GEO (GSE31477).

### Immunoprecipitation of mononucleosomes

Mononucleosome preparation and immunoprecipitation were performed essentially as described (30). The 293T ( $3 \times 10^7$ ) cells were suspended in 2 ml of buffer I [15 mM Tris-HCl, pH 7.5, 300 mM sucrose, 15 mM NaCl, 60 mM KCl, 5 mM MgCl<sub>2</sub>, 0.1 mM EDTA, 10 mM sodium butyrate, 1 mM dithiothreitol (DTT)]. The cell suspension was mixed with buffer II (buffer I containing 0.5% NP-40) by gentle vortexing and incubated for 10 min on ice. Cell lysates were loaded on 8 ml of a 40% sucrose cushion (buffer III: buffer I containing 1.2 M sucrose) and centrifuged at 10 000 rpm for 20 min at 4°C. The pellet of nuclei was resuspended in 1 ml of MNase digestion buffer (50 mM Tris-HCl, pH 7.5, 320 mM sucrose, 4 mM MgCl<sub>2</sub>, 1 mM CaCl<sub>2</sub>, 10 mM sodium butyrate) with 50 U of MNase/ml (Takara) and incubated at 37°C for 20 min. The digestion was stopped by adding 10 mM EDTA and incubating on ice for 15 min, centrifuged at 10 000 rpm for 10 min and the supernatant (S1) was saved. The concentration of nucleosomal DNA was determined using a NanoDrop (Thermo Scientific), and the size of nucleosomal DNA was monitored on an agarose gel after incubation with RNase A and 1% SDS at 37°C for 1 h. The isolated mononucleosomes were diluted 10-fold with FLAG lysis buffer (50 mM Tris-HCl, pH 8.0, 137 mM NaCl, 1 mM EDTA, 1% Triton X-100, 0.2% Sarkosyl, 10% glycerol), immunoprecipitated with anti-H3K4ac antibody and analyzed by immunoblot.

### RNA-seq analysis

RNA-seq analysis was performed as previously described (31). Total RNAs were purified using an RNeasy Plus Kit (Qiagen). RNA-seq libraries were prepared using a SMARTer Stranded Total RNA-seq Kit (Clontech) and sequenced as 101 bp paired-end reads on a HiSeq 2500 or NovaSeq 6000 (Illumina). RNA-seq reads were processed using Trimmomatic and aligned to the human reference genome (hg19). Gene expression levels were quantified as fragments per kilobase of transcript per million mapped reads (FPKM). Differentially expressed genes were determined with the cut-off of FDR < 0.05 and fold change > 1.5. Volcano, scatter and violin plot analyses were performed using R software package.

### Gene set enrichment analysis (GSEA)

GSEA was performed as previously described using the GSEA software package with the gene sets in the Molecular Signatures Database (MSigDB) and target gene sets for Wnt/ $\beta$ -catenin (21), PROX1 (32), MACC1 (22,33), mutant p53 (34) and DBC1 (1098 differentially expressed genes between SW480 WT and D1KO; 840 differentially expressed genes between HCT116 WT and D1KO).

### Real-time quantitative reverse transcription-PCR (qRT-PCR)

Total RNA was purified using TRIzol (Invitrogen), and qRT-PCR was performed with the One-step PrimeScript RT-PCR Kit (Takara). Data were normalized to glyceraldehyde 3-phosphate dehydrogenase (GAPDH) mRNA levels.

The primers used in qRT-PCR are listed in Supplementary Table S5.

### Protein-protein interaction assay

For co-immunoprecipitation (CoIP) assays, cells were lysed with FLAG lysis buffer and immunoprecipitated with specific antibodies or control normal IgG and Protein A/G Plus-Agarose. Glutathione *S*-transferase (GST) pull-down assays were performed using recombinant GST proteins bound to glutathione-agarose beads and *in vitro* translated proteins in NETN buffer (20 mM Tris-HCl, pH 7.6, 150 mM NaCl, 1 mM EDTA, 0.01% NP-40). Bound proteins were analyzed by SDS-PAGE or Tris-Acetate-PAGE (for KMT2D detection) and immunoblot.

### *In vitro* HMT and HAT assay

HA-KMT2D and FLAG-DBC1 proteins were immunopurified from 293T cells transfected with pCMV-HA-KMT2D or p3×FLAG.CMV10-DBC1 by lysis in FLAG lysis buffer followed by immunoprecipitation with anti-HA-agarose or anti-FLAG M2-agarose, washing with FLAG-lysis buffer and elution in Tris-buffered saline (TBS; 50 mM Tris-HCl, pH 7.4, 150 mM NaCl) containing 10% glycerol and HA peptide or 3×FLAG peptide (Sigma-Aldrich). Immunopurified proteins were quantified by immunoblot using anti-HA or anti-FLAG. HA-KMT2D protein was incubated with recombinant nucleosomes (BPS Bioscience) in the presence or absence of FLAG-DBC1 in HMT buffer (50 mM Tris-HCl pH 8.5, 50 mM NaCl, 1 mM DTT, 5% glycerol) supplemented with 30  $\mu$ M *S*-adenosylmethionine (SAM, Sigma-Aldrich) at 30°C for 4 h. For HAT assays, bacterially expressed and purified GST-p300-Br-HAT or GST-CBP-Br-HAT protein was incubated with recombinant nucleosomes with or without GST-DBC1 in HAT buffer [50 mM Tris-HCl pH 8.0, 50 mM KCl, 0.1 mM EDTA, 1 mM DTT, 1 mM phenylmethylsulfonyl fluoride (PMSF), 10 mM sodium butyrate, 5% glycerol] with 30  $\mu$ M acetyl-CoA (Sigma-Aldrich) at 30°C for 10–180 min. For HAT and HMT assays using immunopurified DBC1, the reaction mixture was incubated for 12 h. For HAT-HMT combined *in vitro* assays, GST-p300-Br-HAT and HA-KMT2D or FLAG-KMT2D SET proteins were incubated with or without GST-DBC1 in HMT buffer supplemented with 30  $\mu$ M acetyl-CoA and 30  $\mu$ M SAM at 30°C for 1–4 h. For the inhibition of HAT or HMT activity, 10  $\mu$ M SGC-CBP30 (Selleckchem) or OICR-9429 (Tocris), respectively, was added to the reaction. Reactions were subjected to Bis-Tris PAGE or 4–20% gradient SDS-PAGE and analyzed by immunoblot.

### Proximity biotinylation assay

Proximity biotinylation assays were performed following previously described protocols (35). Briefly, SW480 WT and D1KO cells were transfected with 3×FLAG-tagged TurboID-KMT2D SET or 3×FLAG-tagged TurboID, treated with or without 50  $\mu$ M biotin for 14 h and lysed with FLAG lysis buffer. Biotinylated endogenous proteins were pulled down using streptavidin-agarose (Thermo Scientific) and analyzed by immunoblot.

## RESULTS

### Genome-wide landscape of active enhancer and promoter marks and their association with gene expression in CRC cells

To investigate the epigenomic profiles of AE and AP marks in CRC cells, we performed ChIP-seq in SW480 cells, one of the most commonly used human CRC cell line models. We also included H3K4ac, which was found associated with APs in yeast but has not been well studied in cancer cells (36), and investigated its role in regulation of gene expression. We first confirmed the specificity of antibodies used in ChIP-seq experiments by immunoblot, dot blot and immunoprecipitation assays using nuclear extracts, synthetic H3 peptides with different modifications and site-specifically acetylated recombinant H3 proteins (Supplementary Figure S1). We next identified genomic regions marked by H3K4me3, H3K4me1, H3K4ac, H3K27ac and H3K9/K14ac, and analyzed the genome-wide distribution and Pearson correlation of active histone marks (see Supplementary Table S1 and Supplementary Figures S2A–C and S3A, B for detailed results). We identified 25442 genomic regions co-marked by H3K4me1 and H3K27ac, which demarcate AEs (Supplementary Figure S2D, E), and also found 14255 APs which are marked by both H3K4me3 and H3K9/K14ac (Supplementary Figure S2F). Interestingly, the majority of AEs and APs were co-marked by H3K4ac (Supplementary Figure S3C, D), suggesting that, like H3K27ac (Supplementary Figure S2G), H3K4ac is preferentially associated with APs and AEs.

To investigate the correlation between histone modifications and gene expression levels, we performed RNA-seq analysis in SW480 cells, divided gene expression levels into quartiles according to their FPKM and performed the integrated analysis of ChIP-seq and gene expression data. As expected, AP and AE marks including H3K4ac were present preferentially in highly expressed genes, and their levels were highly correlated with gene expression levels (see Supplementary Figures S2H, I and S3E, F for detailed results), confirming their roles in gene activation.

To investigate whether H3K4ac co-occurs with specific active marks on the same nucleosome, we immunoprecipitated mononucleosomes purified from 293T cells with the H3K4ac antibody and probed with specific histone modification antibodies (Supplementary Figure S3G). H3K4ac-containing mononucleosomes were greatly enriched for H3K27ac and H3K9ac. Interestingly, H3K4me1 and H3K4me3 were also highly enriched in H3K4ac-containing mononucleosomes, indicating that H3K4ac can co-occur with H3K4me1/3 on the same nucleosome. In addition, similar to H3K27ac, H3K4ac was highly enriched and efficiently acetylated by p300 on H3.3, an H3 variant associated with active chromatin, compared with the canonical H3, H3.1 (Supplementary Figure S3H). Because H3K27ac is the most highly enriched active mark in H3K4ac-associated chromatin regions and nucleosomes (Supplementary Figure S3A, G), we tested whether H3K4ac cross-talks with H3K27ac. p300-Br-HAT acetylated H3 robustly on H3K27 and H3K4, and their acetylation was blocked by K-to-R mutation (K27R and K4R) (Supplementary Figure S3I, J). Intriguingly, K27R mutation led to a considerable reduction in H3K4ac levels,

while K4R mutation did not affect H3K27ac levels. In addition, *in vitro* HAT assays using unmodified or site-specifically acetylated (at H3K27) H3 showed that H3K4ac was increased when H3K27 was acetylated (Supplementary Figure S3K), indicating that H3K27ac occurs prior to and facilitates H3K4ac. Together, these results suggest that H3K4ac is globally associated with features and marks of active chromatin and preferentially localized to APs and AEs.

### DBC1 is required for establishing the active chromatin landscape

Although DBC1 has been reported to act as a critical regulator of epigenetic modifiers and TFs, it remains unclear if DBC1 has a direct role in chromatin regulation. To investigate the role of DBC1 in the regulation of histone modifications and gene expression, we performed ChIP-seq for active histone marks in SW480 D1KO cells. Knock-out of DBC1 did not significantly affect global levels of H3 and its modifications (Supplementary Figure S4A). However, DBC1 loss resulted in genome-wide dysregulation of enhancer and promoter marks (Figure 1A–E). Differential peak analysis identified ~2–5 times more regions with decreased (loss) than with increased (gain) levels of H3K4me3, H3K4me1, H3K4ac, H3K27ac and H3K9/K14ac in D1KO cells compared with SW480 WT cells (Figure 1F and Supplementary Figure S4B). To confirm these results in another independent colon cancer cell line, we generated a DBC1 knock-out HCT116 cell line (Supplementary Figure S5) and repeated ChIP-seq experiments in HCT116 cells (Supplementary Figure S6A, B). The enhancer and promoter marks (H3K27ac and H3K4me3) were also dysregulated upon DBC1 loss in HCT116 cells (Supplementary Figure S6C–F). These results suggest a critical role for DBC1 in regulating acetylation and methylation marks on H3. Interestingly, when we overlaid H3K4ac signals with DBC1-regulated active marks, we confirmed co-occupancy of H3K4ac with enhancer and promoter marks and found a concordant decrease and increase in H3K4ac signal at lost and gained regions, respectively, of enhancer and promoter marks (Figure 1A–E), again indicating the association of H3K4ac with gene activation. Importantly, DBC1 loss impaired > 40% of AEs (Figure 1G, H) and also resulted in significant alterations in levels of AE-associated H3K4me3 (24%), H3K4ac (35%) and H3K9/K14ac (42%) (Supplementary Figure S4C), suggesting that DBC1 is required for establishing the AE landscape and for epigenetic regulation of histone modifications in CRC cells.

### DBC1-regulated histone modifications are associated with transcriptional programs involved in CRC progression

To identify DBC1-regulated gene expression programs in CRC cells, we performed RNA-seq analyses using SW480 WT and D1KO cells. A total of 1098 genes were differentially expressed in SW480 D1KO compared with WT cells, with 645 down-regulated and 453 up-regulated genes (Figure 2A). Consistent with our previous microarray-based study (21,22), GSEA showed significant down-

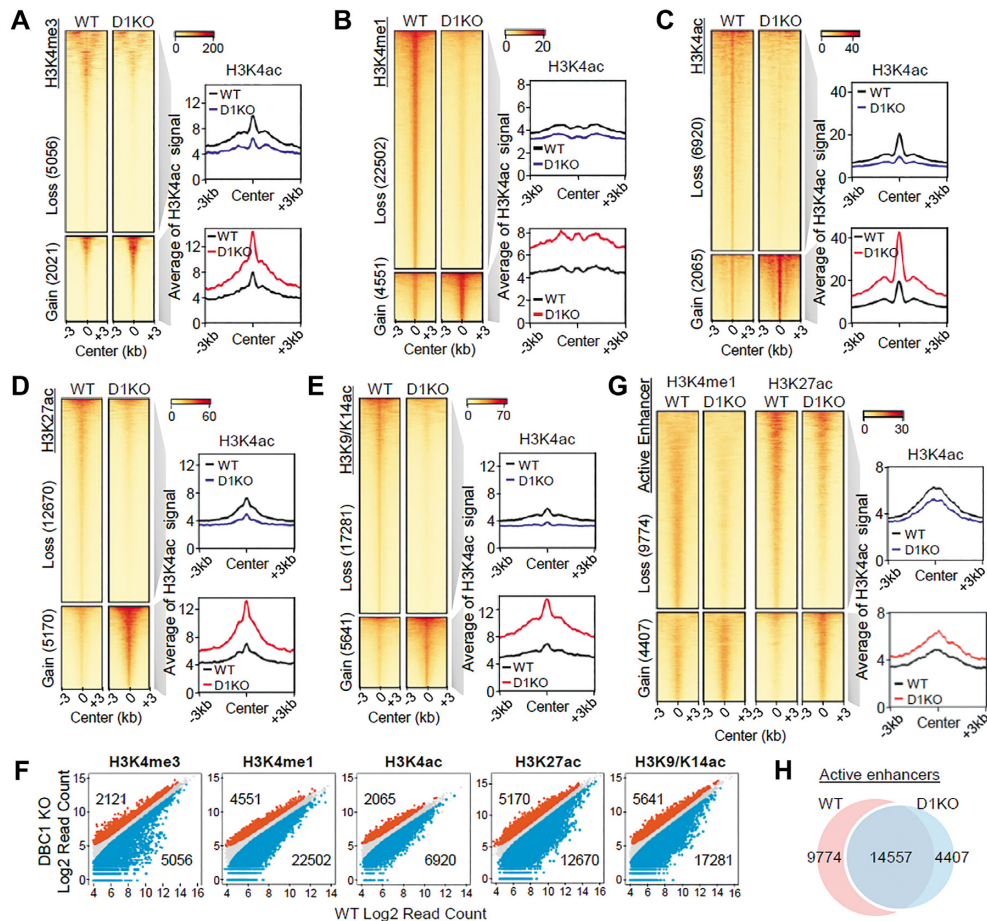


**Figure 1.** DBC1 regulates the epigenetic landscape of active histone modifications. (A–E) Heatmap representations of ChIP-seq signals of H3K4me3 (A), H3K4me1 (B), H3K4ac (C), H3K27ac (D) and H3K9/K14ac (E) in SW480 WT versus D1KO cells. Signals within 3 kb around the center of ChIP-seq peaks of each histone modification (loss and gain regions) are ordered by decreasing ChIP-seq signal in WT cells. Right: plots of average ChIP-seq signal of H3K4ac at lost and gained regions of each histone modification. (F) Scatter plots showing changes in ChIP-seq signals for H3K4me3, H3K4me1, H3K4ac, H3K27ac and H3K9/K14ac in SW480 WT versus D1KO cells (blue, lost in WT cells; red, gained in D1KO cells). Cut-off:  $\log_2\text{FC} > 0.58$  and  $P < 0.05$  by MANorm. (G) Heatmap of H3K4me1 and H3K27ac at AEs in SW480 WT versus D1KO cells. Right: plots of average H3K4ac ChIP-seq signal at lost and gained AEs. (H) Venn diagram showing overlap between AEs in SW480 WT and D1KO cells.

regulation of the expression of Wnt/ $\beta$ -catenin, PROX1 and MACC1 target genes in DBC1 KO cells (Figure 2B). In addition, further GSEA using Hallmark gene sets revealed that loss of DBC1 leads to down-regulation of gene expression programs involved in CRC progression and metastasis [e.g. epithelial–mesenchymal transition (EMT), IL2/STAT5, Wnt/ $\beta$ -catenin, angiogenesis, mutant p53 targets and glycolysis] (Figure 2C). These results were confirmed by RNA-seq analysis in HCT116 WT and D1KO cells (Supplementary Figure S7A–C), suggesting a critical role for DBC1 in gene activation involved in CRC progression. To identify direct targets of DBC1, we performed ChIP-seq for DBC1 in SW480 cells (Supplementary Figure S13A). We identified a total of 10097 DBC1 ChIP-seq peak regions, which were annotated to 6858 genes (Supplementary Table S2). Integration of ChIP-seq and RNA-seq data revealed that of the 1098 DBC1-regulated genes, 447 genes (40.7%) were direct targets (267/645 DBC1 knock-out down-regulated genes and 180/453 DBC1 knock-out up-regulated genes) with DBC1-occupied sites (Figure 2D,

E), suggesting that DBC1 can regulate global gene expression directly and indirectly.

To investigate the correlation between DBC1-regulated histone modifications and gene transcription, we performed the integrated analysis of our ChIP-seq and RNA-seq data. The levels of H3K4me3, H3K4me1, H3K4ac, H3K27ac and H3K9/K14ac were coordinately decreased and increased in the down-regulated and up-regulated gene sets, respectively, by DBC1 knock-out in SW480 cells, and directions of changes in active marks and gene expression caused by DBC1 loss were positively correlated with Pearson correlation coefficients from 0.59 to 0.76 ( $P < 2.2E-16$ ) (Figure 2F). We also obtained comparable results in HCT116 cells for H3K27ac and H3K4me3 (Supplementary Figure S7D). In addition, lost and gained enhancers in D1KO cells were associated with down-regulated and up-regulated genes, respectively (Figure 2G). Together, these results suggest that DBC1 is required for the establishment of active epigenetic modifications and transcriptional activation of genes involved in CRC progression.

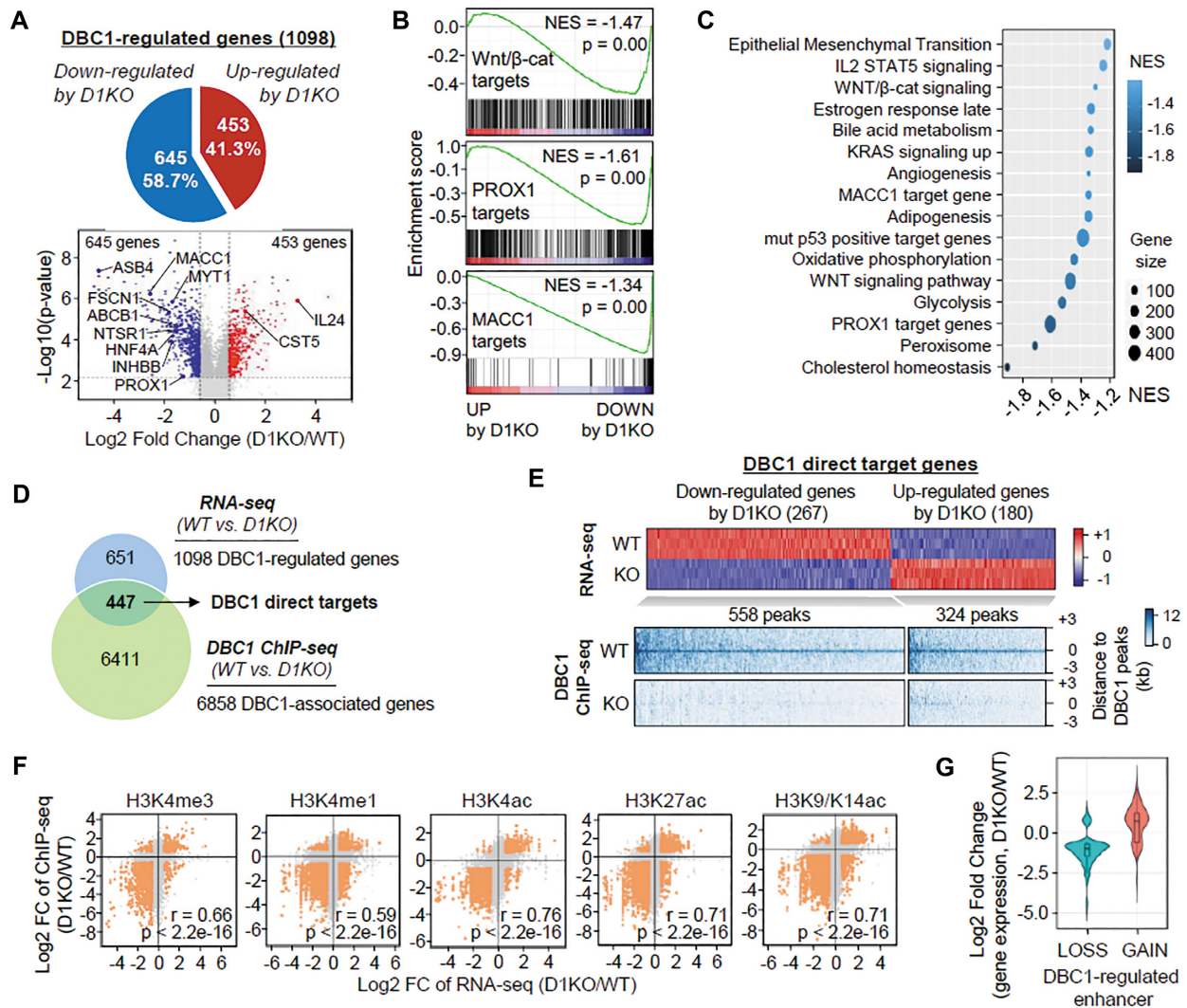


**Figure 2.** DBC1-mediated active histone modifications are required for transcriptional activation of genes involved in cancer progression. (A) RNA-seq analysis of differential gene expression in SW480 cells upon DBC1 knock-out. Pie and volcano plots show that 1098 genes are differentially expressed in SW480 WT versus D1KO cells. Cut-off: log<sub>2</sub>FC > 0.58 and FDR < 0.05. (B) GSEA showing negative enrichment of Wnt/ $\beta$ -catenin, PROX1 and MACC1 target gene signatures in SW480 D1KO cells compared with WT cells. NES, normalized enrichment score. (C) GSEA of top enriched Hallmark gene sets in SW480 WT versus D1KO cells. (D) Venn diagram showing the overlap of DBC1-associated genes (ChIP-seq) and DBC1-regulated genes (RNA-seq). A total of 447 genes in the overlap are identified as DBC1 direct target genes. (E) Heatmaps showing the pattern of DBC1 direct target gene expression. Of the DBC1 direct targets, 267 and 180 genes were down-regulated and up-regulated, respectively, in SW480 D1KO cells compared with WT cells. (F) Scatter plots of Pearson correlation between log<sub>2</sub>FC in gene expression and active histone marks in SW480 cells upon DBC1 knock-out. (G) Violin plots with boxplots inside showing log<sub>2</sub>FCs in gene expression that are regulated by lost and gained enhancers in SW480 cells upon DBC1 knock-out.

### DBC1 plays a critical role in regulating the SE landscape and SE-associated gene expression

Cancer-specific SEs have been identified as key drivers of dysregulated gene expression in several types of cancers including CRC (4,5). In addition, super-enhancer RNAs (seRNAs) transcribed from SEs have also been reported to contribute to tumorigenesis by promoting oncogene expression, cancer cell proliferation and EMT (37). To determine the SE landscape and SE-associated genes in CRC cells and investigate a potential role for DBC1 in regulating SEs, we used the ROSE algorithm based on the H3K27ac (a hallmark of SEs) ChIP-seq datasets. When ranked by the H3K27ac ChIP-seq signal enrichment, 845

and 601 SEs were identified with 771 and 547 potential target genes in SW480 WT and D1KO cells, respectively (Figure 3A). Pathway enrichment analysis using Hallmark gene sets revealed that SE-associated genes in SW480 WT are enriched in pathways involved in CRC progression such as Wnt/ $\beta$ -catenin, TNF $\alpha$ , TGF $\beta$ , EMT and KRAS signaling (Supplementary Figure S8A). Notably, a majority of SEs (76%, 643/845) were located in transcription start site (TSS)-proximal enhancer regions (Supplementary Figure S8B), and TSS-proximal SEs were highly enriched for H3K4ac and H3K4me3 (Supplementary Figure S8C). Because H3K27ac facilitates H3K4ac, we next asked whether H3K4ac can also identify SEs. Using the ROSE algorithm based on the H3K4ac ChIP-seq signal,

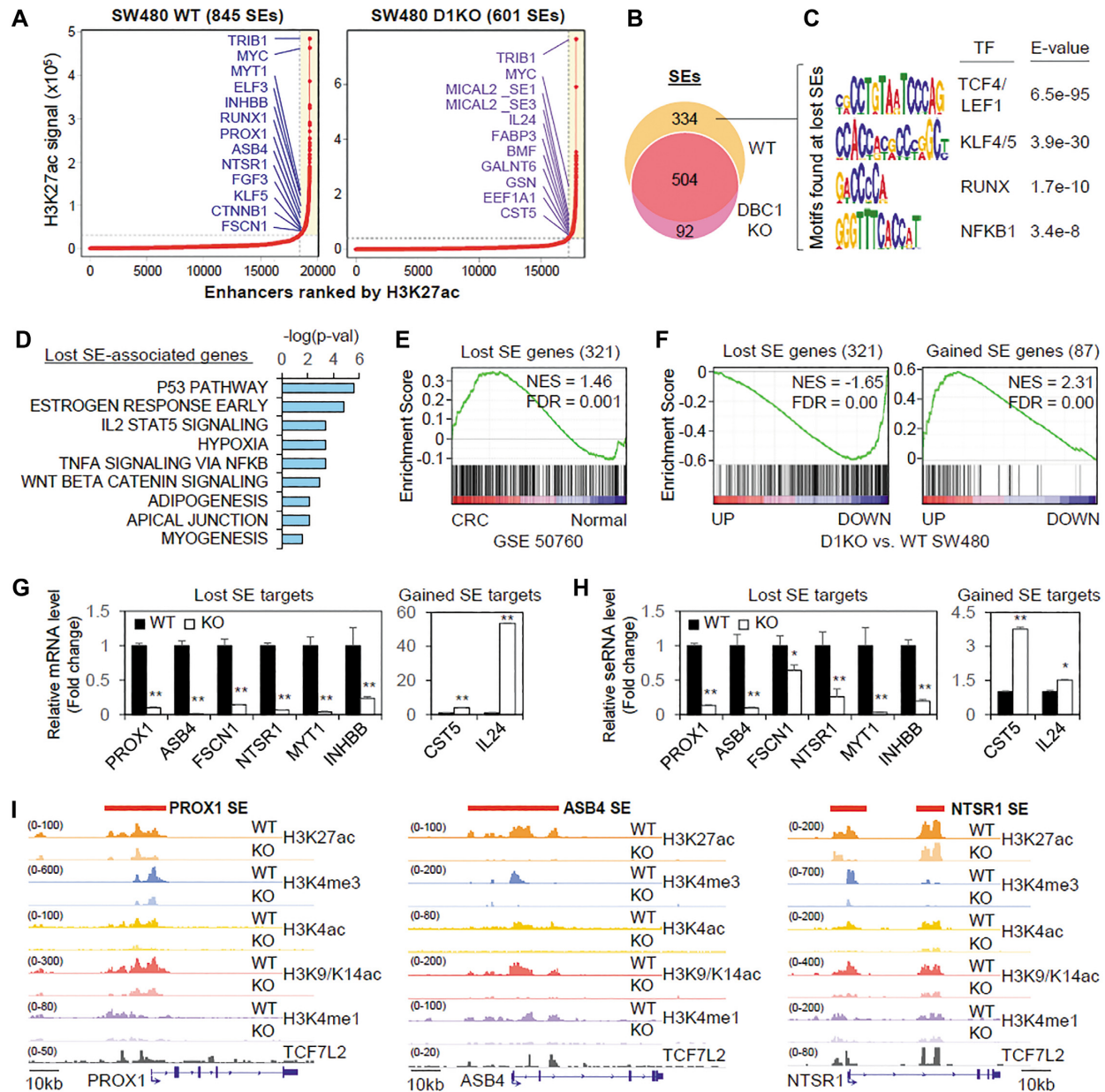


**Figure 3.** DBC1 is required for SE-associated gene expression in CRC cells. (A) Identification of SEs based on H3K27ac ChIP-seq signals in SW480 WT and D1KO cells using the ROSE algorithm. (B) Venn diagram showing the intersection of SEs identified in SW480 WT and D1KO cells. (C) MEME-ChIP motif analysis reveals the top enriched motifs within lost SEs in SW480 D1KO cells. (D) Bar plot showing enriched Hallmark pathways for 321 lost SE-associated genes in SW480 D1KO cells. (E) GSEA of gene expression in human CRC versus normal colon tissues (GSE50760) using the lost SE-associated gene set. (F) GSEA showing negative and positive enrichment of lost and gained SE-associated gene sets, respectively, in SW480 D1KO compared with WT cells. (G, H) qRT-PCR analyses of mRNA (G) and seRNA (H) expression of lost and gained SE-associated genes in SW480 WT and D1KO cells. Data are expressed as fold change relative to the WT and are means  $\pm$  SD ( $n = 3$ ). (I) Snapshots of ChIP-seq tracks for H3K27ac, H3K4me3, H3K4ac, H3K9/K14ac, H3K4me1 and TCF7L2 at SEs of PROX1, ASB4 and NTSR1 genes in SW480 WT and D1KO cells.

we identified 627 SEs in SW480 WT cells, 93.3% of which were overlapped with H3K27ac-enriched SEs (Supplementary Figure S9A, B). Pathway analysis of genes associated with H3K4ac-enriched SEs showed similar results to those obtained with H3K27ac SE-associated genes (Supplementary Figure S9C), suggesting together that H3K4ac can identify SEs in CRC cells. Importantly, 40% (334/845) and 41% (259/627) of H3K27ac SEs and H3K4ac SEs, respectively, in SW480 WT cells were lost in D1KO cells

(Figure 3B and Supplementary Figure S9D), suggesting a critical role for DBC1 in regulating the SE landscape in CRC cells. Similar results of SE analysis were observed in HCT116 WT and D1KO cells (Supplementary Figure S10). The enriched TF motifs at the lost SEs in D1KO cells include those bound by TCF4/LEF1, NF $\kappa$ B, RUNX and KLF4/5 (Figure 3C), suggesting that DBC1 loss may down-regulate transcriptional programs regulated by these CRC-related TFs. Indeed, lost SE-associated genes were enriched

in pathways associated with CRC progression, including Wnt/ $\beta$ -catenin/TCF4 and TNF $\alpha$ /NF $\kappa$ B signaling (Figure 3D), and also in genes highly expressed in CRC tissues compared with normal colon tissues (Figure 3E and Supplementary Figure S8D). Further GSEA showed a significant decrease in the expression of genes associated with lost SEs and an increase in the expression of genes associated with gained SEs in D1KO cells (Figure 3F and Supplementary Figure S9E). These results were confirmed by qRT-PCR, which showed that mRNA levels of lost and gained SE target genes were decreased and increased, respectively, in D1KO cells (Figure 3G), concomitant with a decrease and increase in their seRNA levels (Figure 3H). By analyzing publicly available ENCODE ChIP-seq datasets, we found that TCF4/TCF7L2 densely occupies the SE regions of PROX1, ASB4, NTSR1, FSCN1, INHBB and MYT1 genes, which were overlapped with H3K27ac peaks (Figure 3I and Supplementary Figure S8E). Interestingly, in addition to H3K27ac and H3K4ac SE marks, H3K4me3, H3K4me1 and H3K9/K14ac were also associated with the SE regions, and DBC1 loss markedly reduced their levels at TCF4-occupied SE regions (Figure 3I and Supplementary Figure S8E). These results suggest that DBC1 plays a pivotal role in SE activation and SE-associated gene expression through not only facilitating SE formation and seRNA expression but also maintaining active histone marks at SE regions.

#### DBC1 interacts with and positively regulates histone-modifying activities of p300 and KMT2D

To investigate the mechanism by which DBC1 regulates histone modifications, we performed HAT and HMT assays using recombinant nucleosomes and FLAG-tagged DBC1 immunoprecipitated from SW480 cells transfected with FLAG-DBC1. DBC1 immunoprecipitates had high levels of HAT and HMT activities, which acetylate H3K27 and H3K4 and methylate H3K4 (H3K4me1/2/3) (Figure 4A, B), suggesting that DBC1 is physically associated with HAT and HMT activities in CRC cells. Indeed, FLAG-DBC1 immunoprecipitates contained p300 and KMT2D, which are major epigenomic writers for enhancer marks (Figure 4C), and endogenous CoIP experiments in SW480 cells confirmed the association of DBC1 with p300 and KMT2D (Figure 4D). GST pull-down assays mapped the DBC1 interaction domain of KMT2D and p300 to the catalytic SET and HAT domains, respectively (Figure 4E and Supplementary Figure S11A–C) and showed that the N-terminal domain (NTD) of DBC1 is necessary and sufficient for binding to KMT2D SET and p300 HAT domains (Supplementary Figure S11D, E).

Because DBC1 directly interacts with catalytic domains of KMT2D and p300, we next investigated whether DBC1 can regulate their histone-modifying activities. 293T cells were transfected with plasmids expressing FLAG-H3, HA-p300-Br-HAT and FLAG-DBC1, and acetylated levels of H3K27 and H3K4 were determined by immunoblots. DBC1 overexpression strongly increased p300-mediated H3K4ac and H3K27ac (Figure 4F). *In vitro* time-course HAT assays confirmed enhancement of both p300 and CBP HAT activity by DBC1 (Supplementary Figure S12A,

B), indicating that DBC1 can enhance the HAT activity of both p300 and CBP, and further showed that, consistent with the conclusion in Supplementary Figure S3I–K, H3K27ac precedes H3K4ac. In addition, we also found in *in vitro* HMT assays using immunopurified HA-KMT2D and FLAG-DBC1 that DBC1 enhances KMT2D-mediated H3K4me1/2/3 (Figure 4G). Consistent with protein–protein interaction data (Supplementary Figure S11D, E), the NTD of DBC1 is functionally required and sufficient to promote the catalytic activities of KMT2D and p300 (Supplementary Figure S12C, D).

We next investigated the mechanisms by which DBC1 promotes the catalytic activity of KMT2D and p300. Given that major components of the KMT2D complex, ASH2L, RBBP5, WDR5 and UTX, are co-immunoprecipitated with DBC1 (Figure 4C) and that the core components are required for efficient HMT activity of KMT2D (12,38), we assessed the effect of DBC1 expression on KMT2D complex formation. Overexpression of DBC1 increased the association of KMT2D with its core components in CoIP experiments (Figure 4H). In contrast, DBC1 loss impaired the association of KMT2D with its endogenous core components (Figure 4I and Supplementary S12E), suggesting that DBC1 acts as a positive regulator of KMT2D by enhancing the HMT activity through facilitating KMT2D complex formation. Autoacetylation of the p300 HAT domain has been shown to increase its catalytic activity (39). We therefore performed *in vitro* and *in vivo* acetylation assays to determine the effect of DBC1 on p300 autoacetylation levels and found that DBC1 enhanced the autoacetylation of the p300 HAT domain (Figure 4J and Supplementary Figure S12F). Moreover, DBC1 loss reduced acetylation levels of endogenous p300 (Figure 4K), suggesting that DBC1 positively regulates p300 HAT activity through enhancing p300 autoacetylation. The NTD of DBC1, which directly binds both KMT2D SET and p300 HAT domains, showed similar effects on KMT2D complex formation (Supplementary Figure S12G) and p300 autoacetylation (Supplementary Figure S12H), demonstrating that the DBC1 NTD is sufficient for promoting KMT2D complex assembly and p300 autoacetylation.

#### DBC1 is required for efficient chromatin binding of KMT2D and p300 and targeted to SEs by TCF4/LEF1

Given the physical and functional association of DBC1 with KMT2D and p300, we next performed ChIP-seq for DBC1, KMT2D and p300 in SW480 WT and D1KO cells to investigate whether DBC1 could co-localize with KMT2D and p300 on chromatin and regulate chromatin binding of KMT2D and p300. We identified 10097, 30642 and 29078 regions bound by DBC1, KMT2D and p300, respectively, in SW480 WT cells (Supplementary Table S2), and the majority of DBC1, KMT2D and p300 binding occurred at promoter and intergenic regions (Supplementary Figure S13B). Integration of ChIP-seq data for DBC1, KMT2D and p300 found 5786 (DBC1<sup>+</sup>KMT2D<sup>+</sup>), 5666 (DBC1<sup>+</sup>p300<sup>+</sup>) and 5384 (DBC1<sup>+</sup>KMT2D<sup>+</sup>p300<sup>+</sup>) DBC1-binding genomic regions co-occupied by KMT2D or/and p300 (Figure 5A, B). Further genomic analysis in conjunction with our SE data identified 1304 DBC1-KMT2D-p300 co-occupied regions

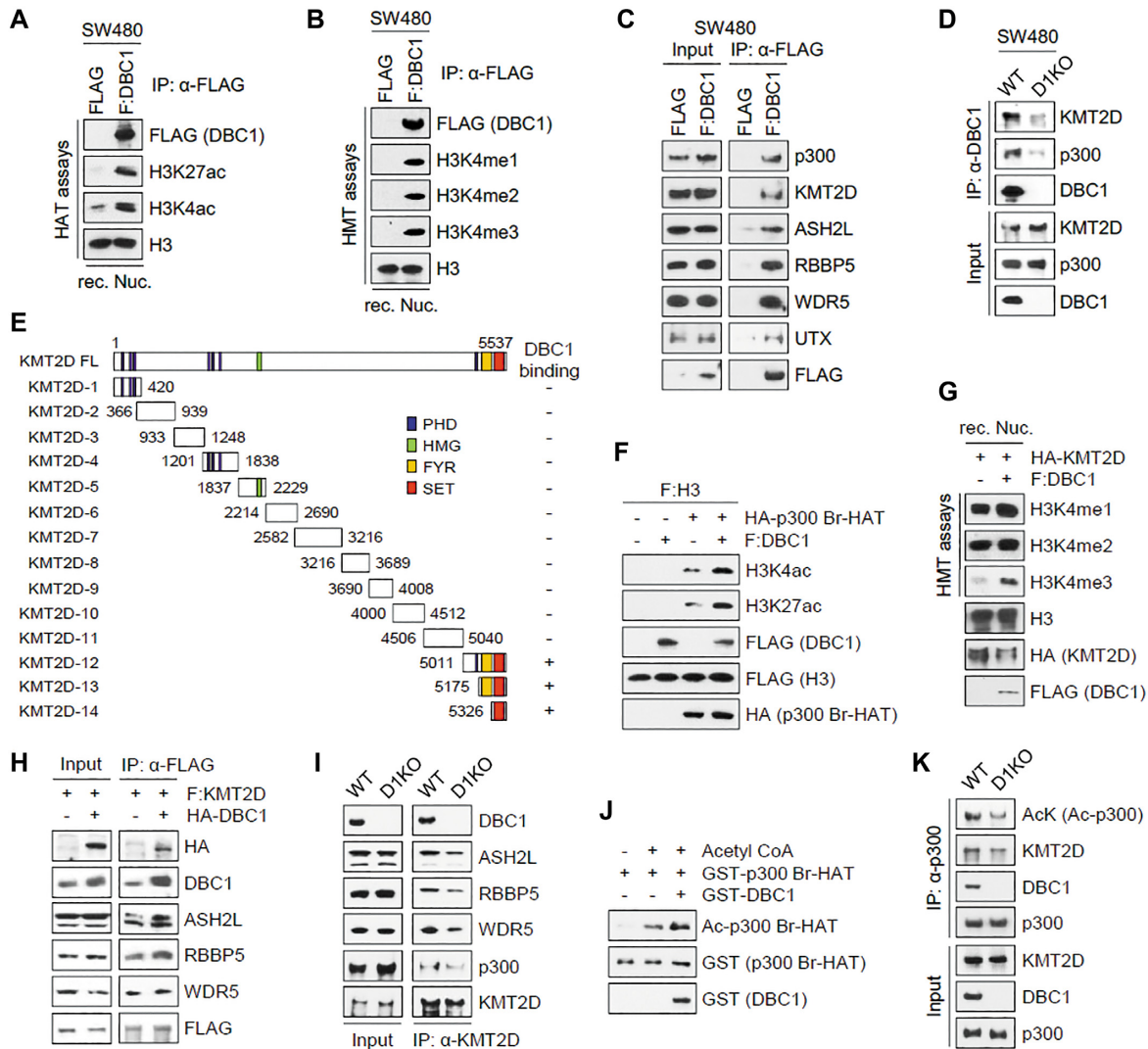


**Figure 4.** DBC1 binds to and enhances the histone-modifying activities of p300 and KMT2D. (A, B) *In vitro* HAT (A) and HMT (B) assays using recombinant nucleosomes and immunopurified FLAG-DBC1 from SW480 cells. HAT and HMT reactions were analyzed by immunoblot using the indicated antibodies. (C) Association of ectopically expressed FLAG-DBC1 with the endogenous p300 and KMT2D complex in SW480 cells. Immunoprecipitation (IP) and immunoblotting were performed using the indicated antibodies. (D) Endogenous CoIP between DBC1 and KMT2D or p300 in SW480 WT and D1KO cells. Immunoprecipitation and immunoblotting were performed using the indicated antibodies. (E) Schematic representation of the KMT2D fragments used in GST pull-down assays and their binding abilities to GST-DBC1 (see also Supplementary Figure S11A). PHD, plant homeotic domain; HMG, high mobility group; FYR, FY-rich domain. (F) 293T cells were transfected with FLAG-H3 along with HA-p300-Br-HAT and/or FLAG-DBC1, and cell lysates were analyzed by immunoblot with the indicated antibodies. (G) *In vitro* HMT assays using recombinant nucleosomes with immunopurified HA-KMT2D from 293T cells transfected with HA-KMT2D and FLAG-DBC1 as indicated. HMT reactions were analyzed by immunoblot using the indicated antibodies. (H) 293T cells were transfected as indicated, and FLAG-KMT2D immunoprecipitates were analyzed by immunoblot with the indicated antibodies. (I) Endogenous CoIP of the indicated core components, DBC1 and p300 with KMT2D in 293T WT and D1KO cells. Immunoprecipitation and immunoblotting were performed using the indicated antibodies. (J) *In vitro* autoacetylation assays of p300-Br-HAT with or without DBC1 as indicated. Acetylation (Ac) levels of p300-Br-HAT were determined by immunoblot using pan-acetyl-lysine (AcK) antibody. (K) Endogenous p300 was immunoprecipitated from SW480 WT and D1KO cells with p300 antibodies, and p300 acetylation levels and CoIPed DBC1 and KMT2D were detected by immunoblot using the indicated antibodies.

(646 SEs, 605 genes) in SEs (Figure 5C). ChIP-seq analyses also revealed that loss of DBC1 resulted in a global redistribution of KMT2D and p300 (Figure 5D), with no measurable effect on their expression levels (Supplementary Figure S13C). Of the KMT2D- and p300-binding regions detected in SW480 WT cells, 8902 KMT2D and 11398 p300 binding sites (29% and 39%, respectively) were lost in D1KO cells, whereas 1499 KMT2D- and 1526 p300-binding sites were gained (Figure 5D and Supplementary Figure S13D).

In addition, 16.1% and 20.8% of KMT2D and p300 ChIP-seq peaks on DBC1<sup>+</sup>KMT2D<sup>+</sup> and DBC1<sup>+</sup>p300<sup>+</sup> regions, respectively, were lost in D1KO cells (Figure 5B). Similarly, DBC1 loss decreased the occupancy of KMT2D and p300 on DBC1-regulated AEs and SEs (Figure 5E). These results suggest a critical role for DBC1 in genome-wide chromatin binding and enhancer recruitment of KMT2D and p300.

Consistent with motif analysis results of the lost SEs in D1KO cells (Figure 3C), the TCF4/LEF1 mo-

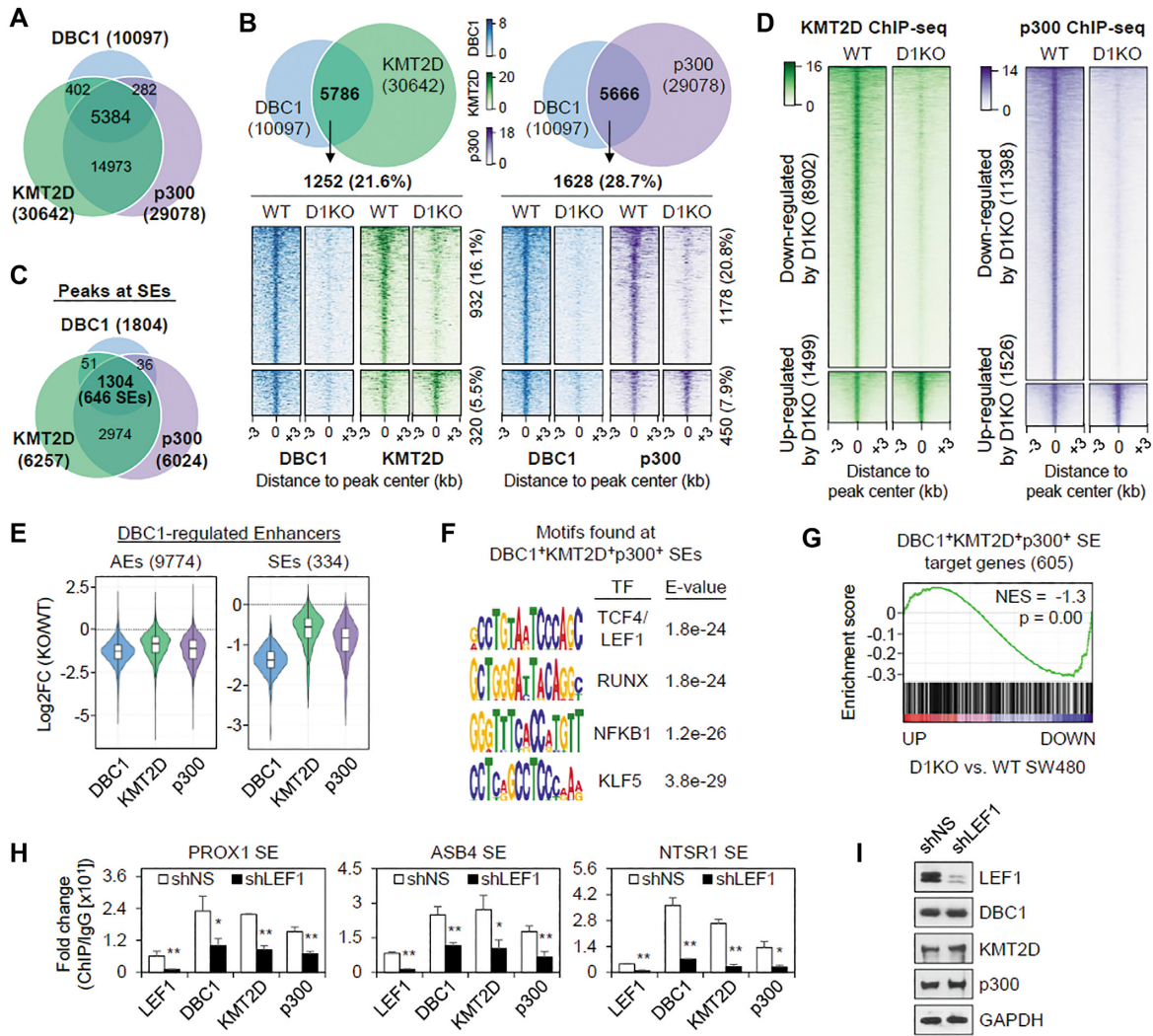


**Figure 5.** DBC1 is required for efficient chromatin binding and enhancer recruitment of KMT2D and p300 and is targeted to SEs by TCF4/LEF1. (A) Venn diagram showing overlap between ChIP-seq peaks for DBC1, KMT2D and p300 on the human genome. (B) Venn diagram showing the genome-wide overlap of DBC1 peaks with KMT2D (upper left) and p300 (upper right). Heatmaps of lost and gained KMT2D and p300 ChIP-seq peaks on DBC1<sup>+</sup>KMT2D<sup>+</sup> (lower left) and DBC1<sup>+</sup>p300<sup>+</sup> (lower right) regions in SW480 WT versus D1KO cells. (C) Venn diagram showing overlap between ChIP-seq peaks for DBC1, KMT2D and p300 at SEs. (D) Heatmaps of lost and gained KMT2D and p300 ChIP-seq signals in SW480 WT versus D1KO cells (see also Supplementary Figure S13D). (E) Violin plots showing changes in KMT2D and p300 occupancy levels on DBC1-regulated AEs (left) and SEs (right) in SW480 WT versus D1KO cells.  $P < 10^{-16}$ . (F) MEME-ChIP motif analysis reveals the top enriched motifs on DBC1<sup>+</sup>KMT2D<sup>+</sup>p300<sup>+</sup> SEs in SW480 cells. (G) GSEA showing that DBC1<sup>+</sup>KMT2D<sup>+</sup>p300<sup>+</sup> SE target genes are enriched among genes down-regulated by D1KO in SW480 cells. (H, I) ChIP-qPCR assays. Sheared chromatin from SW480 cells infected with lentiviruses expressing a control (NS) or LEF1 shRNA was immunoprecipitated with the indicated antibodies. qPCR analyses were performed using primers specific for SEs of the PROX1, ASB4 and NTSR1 genes. ChIP signals were normalized with inputs and shown as fold change relative to control IgG signal and are means  $\pm$  SD ( $n = 3$ ) (H). \* $P < 0.05$ , \*\* $P < 0.01$ . Protein levels were monitored by immunoblot using the indicated antibodies (I).

tif was identified as one of the most significantly enriched motifs on DBC1<sup>+</sup>KMT2D<sup>+</sup>p300<sup>+</sup> SEs (Figure 5F). DBC1<sup>+</sup>KMT2D<sup>+</sup>p300<sup>+</sup> SE target genes were highly enriched in the Wnt/ $\beta$ -catenin pathway (Supplementary Figure S13E), and GSEA revealed a significant reduction in their expression in D1KO cells (Figure 5G). These findings raise the possibility that the Wnt-regulated TF TCF4/LEF1 may modulate the recruitment of DBC1, together with KMT2D and p300, to SEs and that their recruitment mediated by TCF4/LEF1 may be coupled in SE activation. To validate motif analysis and to investigate the role of TCF4/LEF1 in targeting DBC1, KMT2D and p300 to

DBC1<sup>+</sup>KMT2D<sup>+</sup>p300<sup>+</sup> SEs, we performed ChIP-qPCR assays in SW480 cells. Knockdown of LEF1 decreased occupancy not only of LEF1 but also of DBC1, KMT2D and p300 on LEF1-targeted SEs (Figure 5H), while having no effect on their expression levels (Figure 5I), indicating that DBC1, together with KMT2D and p300, is targeted to SEs by the Wnt-regulated TF TCF4/LEF1, which is known to occupy the majority of CRC-driven SEs (10). We have previously shown that DBC1 does not interact directly with LEF1 but can function as a secondary co-activator for LEF1 through its association with  $\beta$ -catenin, which directly binds to and acts as a primary co-activator for LEF1

by recruiting additional co-activators (21,22). These findings suggest that DBC1 is recruited to LEF1-binding sites in chromatin through the interaction with  $\beta$ -catenin. Consistent with this notion, depletion of  $\beta$ -catenin decreased occupancy of DBC1, KMT2D and p300 on the SE of the PROX1 gene, without affecting their cellular levels (Supplementary Figure S13F, G). Altogether, these results suggest that TCF4/LEF1 and  $\beta$ -catenin are required for recruitment of DBC1, KMT2D and p300 to the SEs and that DBC1 plays a critical role in coregulator complex formation on TCF4/LEF1-targeted SEs.

### **DBC1 facilitates SE-associated histone modifications by mediating cooperative functional interactions between p300 and KMT2D**

We next examined the possible cross-talk between H3K4 methylation and H3 acetylation by performing ChIP-qPCR assays in SW480 cells depleted of KMT2D or treated with SGC-CBP30, a selective p300/CBP bromodomain inhibitor. Depletion of KMT2D or treatment with SGC-CBP30 had no effect on cellular levels of p300 or KMT2D, respectively (Figure 6A). However, KMT2D depletion resulted in a great reduction not only in H3K4me1/3 levels but also in H3K27ac and H3K4ac levels on SEs of PROX1, ASB4, FSCN1 and NTSR1 genes (Figure 6B). Similarly, inhibition of p300 with SGC-CBP30 led to a significant decrease in both H3 acetylation and H3K4 methylation (Figure 6B), indicating a bidirectional cross-talk between KMT2D-mediated H3K4 methylation and p300-mediated H3 acetylation on the SEs.

We next investigated the role of DBC1 in the cross-talk between p300 and KMT2D. In HMT assays, KMT2D-mediated H3K4me1/2/3 were synergistically increased with the addition of p300-Br-HAT/acetyl-CoA and further enhanced by DBC1 (Figure 6C and Supplementary Figure S14A, C). Similarly, HAT assays showed that KMT2D-SET dramatically enhanced p300-mediated H3K27ac and H3K4ac in an HMT activity-dependent manner, and their acetylation levels were further increased by DBC1 (Figure 6D and Supplementary Figure S14B, C). In support of these results, p300 and KMT2D associated with each other in reciprocal CoIP experiments (Supplementary Figure S14D, E), and overexpression and knock-out of DBC1 strongly increased and decreased their interaction, respectively, in exogenous CoIP (Figure 6E) and reciprocal endogenous CoIP experiments (Figure 4I, K). Moreover, GST pull-down assays further showed that the KMT2D SET domain binds directly to the p300 Br-HAT domain and that DBC1 increases their interaction (Figure 6F). To further confirm DBC1-dependent KMT2D-p300 interactions, we performed a proximity biotinylation assay, a method for labeling proteins in a proximity-dependent manner (35), using an engineered biotin ligase TurboID fused to the KMT2D SET domain. In this approach, endogenous proteins within a nanometer range of the bait protein (TurboID-KMT2D-SET) are covalently modified with biotin (Supplementary Figure S14F). As shown in Figure 6G, endogenous p300 and DBC1 were in close proximity to the KMT2D SET domain in SW480 cells, and DBC1 loss markedly diminished the close proximity interaction between KMT2D-SET and

p300. Together, these results suggest that DBC1 promotes the functional cooperation between KMT2D and p300 by facilitating their association.

To directly prove that DBC1 can activate SE-associated gene transcription by regulating levels of SE marks, we utilized the CRISPR/dCas9-based genome locus-specific targeting system. We co-expressed dCas9-DBC1 fusion protein with multiple sgRNAs targeting the PROX1 SE in SW480 D1KO cells (Figure 6H). Targeting of dCas9-DBC1 to the PROX1 SE recovered H3K27ac and H3K4ac levels (Figure 6I) and also significantly rescued PROX1 mRNA and protein levels in D1KO cells (Figure 6J, K), indicating direct involvement of DBC1 in the regulation of SE activity. Together, these results suggest that DBC1 contributes to SE-associated histone modifications by facilitating the recruitment and cooperative functions of p300 and KMT2D.

## **DISCUSSION**

One of the hallmarks of cancer development and progression is epigenetic dysregulation of histone modifications, which results in aberrant gene expression, genome instability and *de novo* acquisition of cancer-specific SEs (1,4,5). Thus, the investigation of cancer-related histone marks, cancer-specific SEs, epigenetic modifiers and their regulators, and defining their mechanisms of action are essential for a better understanding of cancer progression and development of therapeutic strategies. H3K4ac was found to be enriched at actively transcribed gene promoters in yeast and human cancer cells and globally increased at gene promoters involved in EMT and metastasis during cancer progression (36,40). Here, we further showed that H3K4ac can identify SEs in CRC cells and is preferentially enriched at APs and AEs as well as on histone variant H3.3. The majority of H3K4ac co-localizes with H3K27ac, and H3K27ac directly facilitates H3K4ac, but not vice versa, indicating a sequential order of acetylation on H3 in activating promoter and enhancer activities. Additionally, H3K4ac/H3K4me3-co-marked genes are highly expressed in CRC cells and enriched in cancer signaling pathways, suggesting a cooperative function of H3K4ac and H3K4me3 in gene activation involved in cancer progression.

Accumulating evidence has indicated that DBC1 functions as a co-regulator for several TFs including p53 and nuclear receptors by negatively regulating repressive epigenetic modifiers such as SIRT1, HDAC3, SUV39H1, MDM2 and CHIP (16,17,19–21,23–26). However, there is a significant gap in our knowledge of DBC1 function in the regulation of histone modifications and chromatin structure. In this study, we extend the current understanding of DBC1-mediated transcriptional activation and epigenetic regulation by identifying DBC1 as a key positive regulator of epigenomic writers KMT2D and p300. Loss of DBC1 caused genome-wide dysregulation of active chromatin marks, a global reduction in chromatin binding of KMT2D and p300, and down-regulation of cancer-associated gene expression programs. DBC1 directly interacts with KMT2D and p300, and enhances their histone-modifying enzyme activities, thereby contributing to establishment of active epigenomic landscapes including AEs

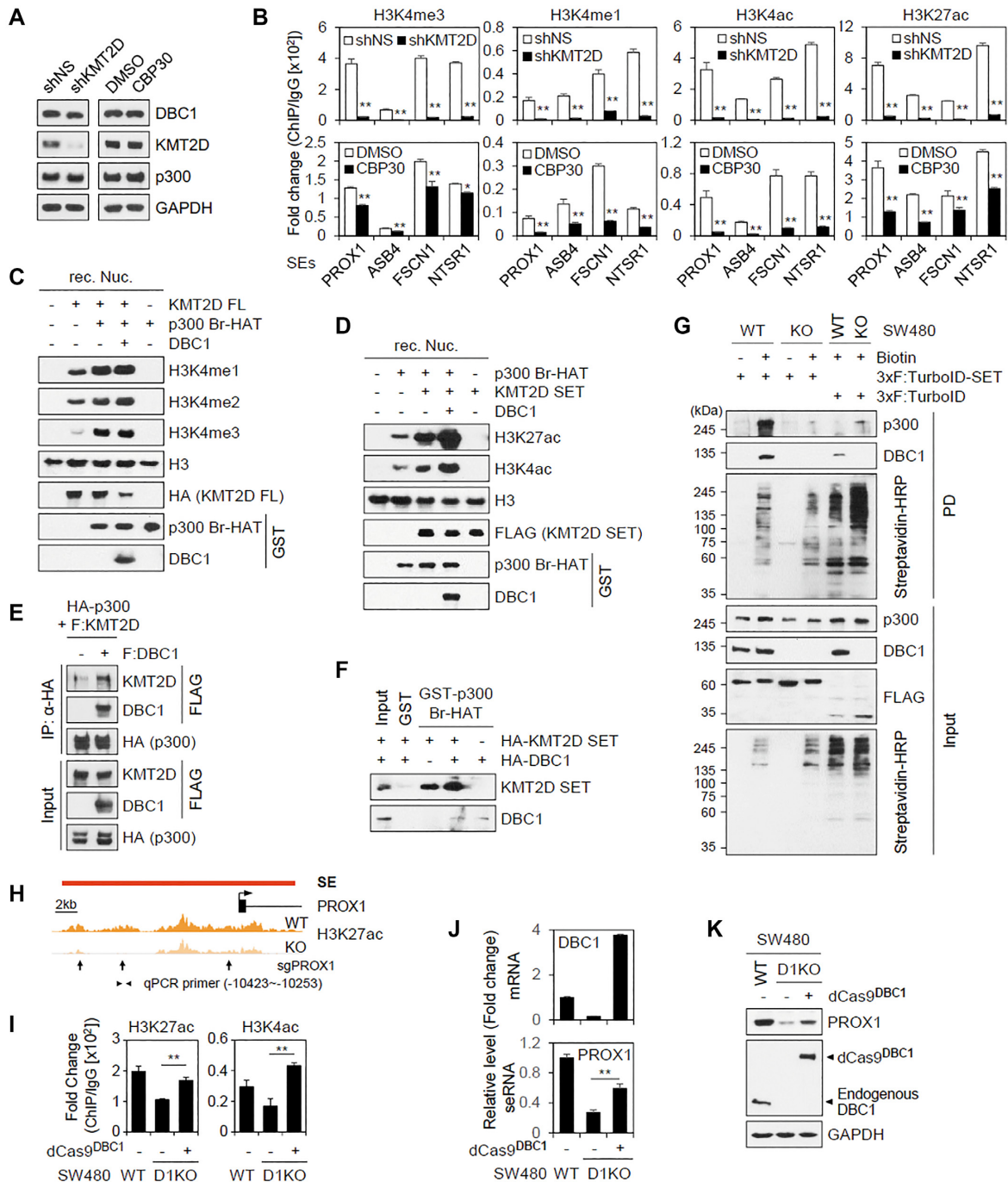


**Figure 6.** DBC1 facilitates SE-associated histone modifications by coordinating the interplay of p300 and KMT2D. (A) Protein levels in SW480 cells depleted of KMT2D or treated with SGC-CBP30 were monitored by immunoblot using the indicated antibodies. (B) ChIP-qPCR assays. Sheared chromatin from SW480 cells infected with lentiviruses expressing either a control (NS) or KMT2D shRNA or SW480 WT cells treated with 5  $\mu$ M SGC-CBP30 for 1 h was immunoprecipitated with the indicated histone modification antibodies. qPCR analyses were performed using primers specific for SEs of the PROX1, ASB4, FSCN1 and NTSR1 genes. ChIP signals were normalized with inputs and shown as fold change relative to control IgG signal, and are means  $\pm$  SD ( $n = 3$ ).  $*P < 0.05$ ,  $**P < 0.01$ . (C, D) *In vitro* HMT assays using recombinant nucleosomes, immunopurified HA-KMT2D, GST-p300-Br-HAT and GST-DBC1 as indicated (C) and *in vitro* HAT assays using recombinant nucleosomes, immunopurified FLAG-KMT2D SET, GST-p300-Br-HAT and GST-DBC1 as indicated (D). The reactions were analyzed by immunoblot using the indicated antibodies. (E) 293T cells were transfected with the indicated constructs, and HA-p300 immunoprecipitates were analyzed by immunoblots with the indicated antibodies. (F) *In vitro* translated HA-KMT2D SET, HA-DBC1 or both were incubated with GST-p300-Br-HAT bound to beads as indicated. Bound proteins were analyzed by immunoblot with anti-HA antibody. (G) Proximity biotinylation assays. SW480 WT and D1KO cells transfected with 3 $\times$ FLAG-TurboID-KMT2D SET or 3 $\times$ FLAG-TurboID were treated with biotin as indicated. Biotinylated endogenous proteins were pulled down using streptavidin beads and analyzed by immunoblot with the indicated antibodies. (H) The PROX1 locus is schematically depicted with locations of H3K27ac peaks in SW480 WT and D1KO, sgRNAs (arrow) and ChIP-PCR primers (arrowhead). (I) SW480 D1KO cells were infected with lentiviruses encoding the dCas9-DBC1 fusion protein and sgRNAs targeting the PROX1 SE. ChIP-qPCR assays using SW480 WT, D1KO and D1KO/dCas9-DBC1 cells were performed with the indicated antibodies.  $**P < 0.01$ . (J) Relative levels of DBC1 mRNA and PROX1 seRNA in SW480 WT, D1KO and D1KO/dCas9-DBC1 cells were determined by qRT-PCR.  $**P < 0.001$ . (K) Protein levels of PROX1 and DBC1 in SW480 WT, D1KO and D1KO/dCas9-DBC1 cells were monitored by immunoblot using the indicated antibodies.

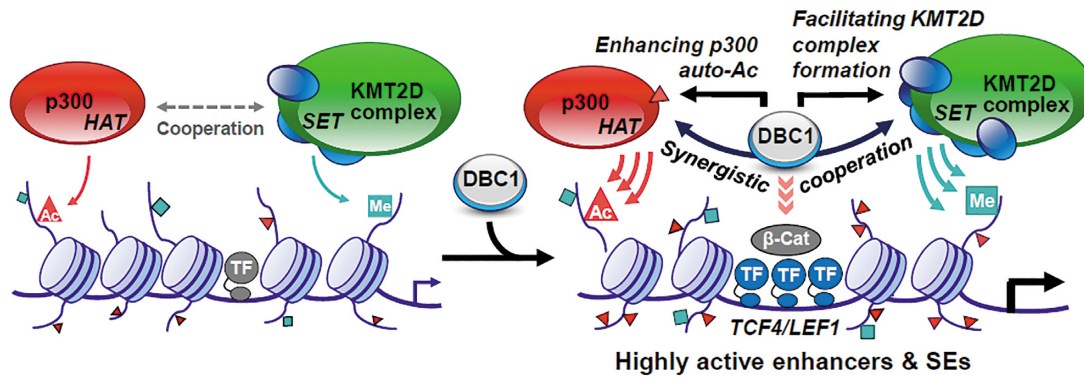


**Figure 7.** A proposed model in which DBC1 plays a critical role in regulating the AE and SE landscapes. DBC1 is targeted to SEs by the Wnt-regulated transcription factor TCF4/LEF1 and  $\beta$ -catenin. DBC1 facilitates the recruitment of and interaction between KMT2D and p300 by directly binding to their catalytic domains (SET and HAT) and promotes independent and cooperative effects of KMT2D and p300 on H3K4 methylation and H3 acetylation by facilitating KMT2D complex formation and enhancing p300 autoacetylation.

and SEs in CRC cells (Figure 7). Moreover, DBC1 can promote the association of KMT2D with its core components and autoacetylation of p300, which are required for their high catalytic activities (Figure 7). These observations could be explained by two non-exclusive mechanisms: DBC1 can either (i) facilitate the rate and/or processivity of KMT2D HMT and p300 HAT activities by promoting KMT2D complex assembly and p300 autoacetylation through direct binding to their catalytic domains or (ii) act by inhibiting repressive epigenetic modifiers (e.g. SIRT1, H3K4 demethylases, H3K9 methyltransferases, etc.). While our results clearly support the first mechanism, it has been reported that DBC1 binds to the catalytic domain of SUV39H1 and inhibits its ability to deposit the repressive methylation mark (H3K9me3) (24). Thus, it is possible that both mechanisms operate simultaneously in cells. In addition, consistent with previous reports that KMT2D is a major H3K4me1/2 methyltransferase (13,14,41), our *in vitro* HMT assays showed that KMT2D has a very weak ability to trimethylate H3K4 compared with its ability to mono- and di-methylate H3K4. Importantly, DBC1 enhanced overall HMT activity of KMT2D for H3K4me1/2/3, supporting our proposed mechanism that DBC1 can promote the processivity and rate of KMT2D-mediated H3K4 methylation.

SEs consist of a large cluster of enhancers typically marked by high levels of H3K27ac, TFs, MED1, BRD4 and enhancer epigenomic writers p300 and KMT2D (4–7). Cancer cells frequently acquire cancer-specific SEs to drive overexpression of oncogenes, which accelerate cancer progression (4,5,37). We found that DBC1 is required for SE formation, recruitment of KMT2D and p300 to SEs, maintenance of active marks on SEs, and SE-associated gene expression in CRC cells. Notably, 72% of DBC1 peaks (1304/1804) in SEs are co-occupied by KMT2D and p300, and DBC1 loss decreased the occupancy of KMT2D and p300 on DBC1-regulated SEs, suggesting that recruitment of the epigenetic writers and DBC1 might be coupled in SE activation. Furthermore, consistent with our previous findings that DBC1 acts as a co-activator for TCF4/LEF1– $\beta$ -catenin-mediated transcription (21,22) and in agreement with a previous report that

CRC-associated SEs are enriched for TCF4/LEF1-binding motifs (8,10), our motif analysis revealed TCF4/LEF1 as the top enriched motif in DBC1-regulated SEs and DBC1<sup>+</sup>KMT2D<sup>+</sup>p300<sup>+</sup> SEs in CRC cells. In addition, LEF1 is indeed required for the recruitment of DBC1, KMT2D and p300 to DBC1<sup>+</sup>KMT2D<sup>+</sup>p300<sup>+</sup> SEs. These findings, together with our previous and current observations that DBC1 enhances TCF4/LEF1– $\beta$ -catenin complex formation on Wnt-regulated enhancers by increasing  $\beta$ -catenin acetylation (21,22) and facilitates recruitment of KMT2D and p300 to SEs and seRNA expression, suggest that DBC1 functions as a pivotal regulator of Wnt/ $\beta$ -catenin signaling through not only regulating acetylation of the non-histone protein  $\beta$ -catenin but also increasing active histone modifications (H3K4 methylation and H3 acetylation) on SEs to establish a favorable epigenetic environment for SE activation.

SET1/KMT2 family HMTs exist in multisubunit complexes containing ASH2L, RBBP5, WDR5 and DPY30, and are often found with other epigenetic modifiers such as HATs and demethylases (12,42,43), and this may be the mechanistic basis of complicated cross-talk between epigenetic marks. Here, we demonstrated physical and functional links between KMT2D and p300 and between their corresponding histone modifications. Previous reports demonstrated that KMT2D is required for the recruitment of p300 and its HAT activity for H3K27 on enhancers activated during adipogenesis and embryonic stem cell differentiation (12–15). p300 was also shown to be required for H3K4 methylation mediated by SET1 and KMT2D complexes (12,44). Furthermore, UTX, a KMT2D-associated H3K27 demethylase, has been shown to facilitate the establishment of the AE landscape in a demethylase activity-independent manner through promoting recruitment and cooperative functional interactions of KMT2D and p300 (12). In line with these previous findings, we found that KMT2D is required not only for H3K4 methylation but also for H3K27ac and H3K4ac on SEs in CRC cells and synergistically increases p300-mediated H3K27ac and H3K4ac in an HMT activity-dependent manner. In addition, we further showed that p300 also increases KMT2D-mediated H3K4me1/2/3 and that its HAT activity is required for

H3K4 methylation on SEs, indicating a strong functional cooperativity between p300 and KMT2D in establishing the SE landscape. Notably, DBC1 enhances cooperative effects of KMT2D and p300 on H3K4 methylation and H3 acetylation. Here we showed several lines of mechanistic evidence of how DBC1, as a key regulator of enhancer epigenomic writers, facilitates cooperativity between KMT2D and p300 (Figure 7): DBC1 not only enhances the respective histone-modifying activities of KMT2D and p300 by facilitating the KMT2D complex assembly and autoacetylation of p300 but also promotes cooperative effects of KMT2D and p300 on H3 acetylation and H3K4 methylation by bringing KMT2D and p300 into close proximity; DBC1 binds a large portion of genomic sites, including SEs, enriched with KMT2D and p300; DBC1 loss impairs genome-wide chromatin binding and SE recruitment of KMT2D and p300, consequently decreasing active histone marks and SE-associated gene expression; targeting DBC1 to the SE of PROX1 recovers PROX1 expression and SE marks (H3K27ac and H3K4ac) on the SE in D1KO cells. Our results firmly establish DBC1 as a key regulator of KMT2D and p300 and provide additional new insights into regulatory mechanisms underlying the functional cooperativity between the enhancer epigenomic writers. Given that DBC1 is associated with the UTX–KMT2D complex (Figure 4C), it will be interesting to investigate whether this function of DBC1 occurs in cooperation with UTX and to assess a role for DBC1 in the UTX–KMT2D–p300 transcriptional regulatory network.

Cancer is a complex disease driven by both genetic and epigenetic changes. A great effort has been made to understand the role of histone modifications in cancer, and emerging evidence suggests that epigenetic alterations in histone modifications and chromatin states drive cancer progression by activating oncogenes and silencing tumor suppressor genes (9). Understanding mechanisms underlying epigenetic alterations in cancer will thus provide useful information to develop novel strategies for epigenetic cancer therapy. Because DBC1 expression is deregulated in various cancers including CRC and is associated with clinical outcomes (20–22,45), our findings may rationalize targeting DBC1 as a promising therapeutic strategy against epigenetically deregulated cancers. In conclusion, our findings highlight the critical role of DBC1 in the interplay between epigenetic modifiers in establishing active chromatin states in CRC cells and suggest that DBC1 is a potential target for epigenetic cancer therapy.

## DATA AVAILABILITY

All sequencing data files (ChIP-seq and RNA-seq) have been deposited at NCBI GEO under SuperSeries accession codes GSE179463 and GSE202478.

## SUPPLEMENTARY DATA

Supplementary Data are available at NAR Online.

## ACKNOWLEDGEMENTS

We thank Dr Laura Pasqualucci (Columbia University) for the HA-KMT2D expression plasmid, and Dr Woojin An

(University of Southern California) for the GST-hH3 expression vector.

## FUNDING

This work was supported by the National Research Foundation of Korea (NRF) grant funded by the Ministry of Science and ICT (MSIT), Republic of Korea [2020R1A2C1009335]; and the Basic Science Research Program through the NRF funded by the Ministry of Education [2019R111A1A01057113].

*Conflict of interest statement.* None declared.

## REFERENCES

- Zhao, S., Allis, C.D. and Wang, G.G. (2021) The language of chromatin modification in human cancers. *Nat. Rev. Cancer*, **21**, 413–430.
- Heintzman, N.D., Stuart, R.K., Hon, G., Fu, Y., Ching, C.W., Hawkins, R.D., Barrera, L.O., Van Calcar, S., Qu, C., Ching, K.A. *et al.* (2007) Distinct and predictive chromatin signatures of transcriptional promoters and enhancers in the human genome. *Nat. Genet.*, **39**, 311–318.
- Guenther, M.G., Levine, S.S., Boyer, L.A., Jaenisch, R. and Young, R.A. (2007) A chromatin landmark and transcription initiation at most promoters in human cells. *Cell*, **130**, 77–88.
- Tang, F., Yang, Z., Tan, Y. and Li, Y. (2020) Super-enhancer function and its application in cancer targeted therapy. *NPJ Precis. Oncol.*, **4**, 2.
- Li, G.H., Qu, Q., Qi, T.T., Teng, X.Q., Zhu, H.H., Wang, J.J., Lu, Q. and Qu, J. (2021) Super-enhancers: a new frontier for epigenetic modifiers in cancer chemoresistance. *J. Exp. Clin. Cancer Res.*, **40**, 174.
- Lovén, J., Hoke, H.A., Lin, C.Y., Lau, A., Orlando, D.A., Vakoc, C.R., Bradner, J.E., Lee, T.I. and Young, R.A. (2013) Selective inhibition of tumor oncogenes by disruption of super-enhancers. *Cell*, **153**, 320–334.
- Whyte, W.A., Orlando, D.A., Hnisz, D., Abraham, B.J., Lin, C.Y., Kagey, M.H., Rahl, P.B., Lee, T.I. and Young, R.A. (2013) Master transcription factors and mediator establish super-enhancers at key cell identity genes. *Cell*, **153**, 307–319.
- Jung, G., Hernández-Illán, E., Moreira, L., Balaguer, F. and Goel, A. (2020) Epigenetics of colorectal cancer: biomarker and therapeutic potential. *Nat. Rev. Gastroenterol. Hepatol.*, **17**, 111–130.
- Flavahan, W.A., Gaskell, E. and Bernstein, B.E. (2017) Epigenetic plasticity and the hallmarks of cancer. *Science*, **357**, eaal2380.
- Hnisz, D., Schuijers, J., Lin, C.Y., Weintraub, A.S., Abraham, B.J., Lee, T.I., Bradner, J.E. and Young, R.A. (2015) Convergence of developmental and oncogenic signaling pathways at transcriptional super-enhancers. *Mol. Cell*, **58**, 362–370.
- Calo, E. and Wysocka, J. (2013) Modification of enhancer chromatin: what, how, and why? *Mol. Cell*, **49**, 825–837.
- Wang, S.P., Tang, Z., Chen, C.W., Shimada, M., Koche, R.P., Wang, L.H., Nakadai, T., Chramiec, A., Krivtsov, A.V., Armstrong, S.A. *et al.* (2017) A UTX–MLL4–p300 transcriptional regulatory network coordinately shapes active enhancer landscapes for eliciting transcription. *Mol. Cell*, **67**, 308–321.
- Wang, C., Lee, J.E., Lai, B., Macfarlan, T.S., Xu, S., Zhuang, L., Liu, C., Peng, W. and Ge, K. (2016) Enhancer priming by H3K4 methyltransferase MLL4 controls cell fate transition. *Proc. Natl Acad. Sci. USA*, **113**, 11871–11876.
- Lee, J.E., Wang, C., Xu, S., Cho, Y.W., Wang, L., Feng, X., Baldrige, A., Sartorelli, V., Zhuang, L., Peng, W. *et al.* (2013) H3K4 mono- and di-methyltransferase MLL4 is required for enhancer activation during cell differentiation. *Elife*, **2**, e01503.
- Lai, B., Lee, J.E., Jang, Y., Wang, L., Peng, W. and Ge, K. (2017) MLL3/MLL4 are required for CBP/p300 binding on enhancers and super-enhancer formation in brown adipogenesis. *Nucleic Acids Res.*, **45**, 6388–6403.
- Kim, J.E., Chen, J. and Lou, Z. (2008) DBC1 is a negative regulator of SIRT1. *Nature*, **451**, 583–586.
- Yu, E.J., Kim, S.H., Heo, K., Ou, C.Y., Stallcup, M.R. and Kim, J.H. (2011) Reciprocal roles of DBC1 and SIRT1 in regulating estrogen

- receptor  $\alpha$  activity and co-activator synergy. *Nucleic Acids Res.*, **39**, 6932–6943.
18. Fu, J., Jiang, J., Li, J., Wang, S., Shi, G., Feng, Q., White, E., Qin, J. and Wong, J. (2009) Deleted in breast cancer 1, a novel androgen receptor (AR) coactivator that promotes AR DNA-binding activity. *J. Biol. Chem.*, **284**, 6832–6840.
  19. Moon, S.J., Jeong, B.C., Kim, H.J., Lim, J.E., Kwon, G.Y. and Kim, J.H. (2018) DBC1 promotes castration-resistant prostate cancer by positively regulating DNA binding and stability of AR-V7. *Oncogene*, **37**, 1326–1339.
  20. Kim, H.J., Kim, S.H., Yu, E.J., Seo, W.Y. and Kim, J.H. (2015) A positive role of DBC1 in PEA3-mediated progression of estrogen receptor-negative breast cancer. *Oncogene*, **34**, 4500–4508.
  21. Yu, E.J., Kim, S.H., Kim, H.J., Heo, K., Ou, C.Y., Stallcup, M.R. and Kim, J.H. (2016) Positive regulation of beta-catenin–PROX1 signaling axis by DBC1 in colon cancer progression. *Oncogene*, **35**, 3410–3418.
  22. Kim, H.J., Moon, S.J., Kim, S.H., Heo, K. and Kim, J.H. (2018) DBC1 regulates Wnt/ $\beta$ -catenin-mediated expression of MACC1, a key regulator of cancer progression, in colon cancer. *Cell Death. Dis.*, **9**, 831.
  23. Chini, C.C., Escande, C., Nin, V. and Chini, E.N. (2010) HDAC3 is negatively regulated by the nuclear protein DBC1. *J. Biol. Chem.*, **285**, 40830–40837.
  24. Li, Z., Chen, L., Kabra, N., Wang, C., Fang, J. and Chen, J. (2009) Inhibition of SUV39H1 methyltransferase activity by DBC1. *J. Biol. Chem.*, **284**, 10361–10366.
  25. Qin, B., Minter-Dykhouse, K., Yu, J., Zhang, J., Liu, T., Zhang, H., Lee, S., Kim, J., Wang, L. and Lou, Z. (2015) DBC1 functions as a tumor suppressor by regulating p53 stability. *Cell Rep.*, **10**, 1324–1334.
  26. Zhao, W., Kruse, J.P., Tang, Y., Jung, S.Y., Qin, J. and Gu, W. (2008) Negative regulation of the deacetylase SIRT1 by DBC1. *Nature*, **451**, 587–590.
  27. Kim, J.H., Yang, C.K. and Stallcup, M.R. (2006) Downstream signaling mechanism of the C-terminal activation domain of transcriptional coactivator CoCoA. *Nucleic Acids Res.*, **34**, 2736–2750.
  28. Kim, J.H., Yang, C.K., Heo, K., Roeder, R.G., An, W. and Stallcup, M.R. (2008) CCAR1, a key regulator of mediator complex recruitment to nuclear receptor transcription complexes. *Mol. Cell*, **31**, 510–519.
  29. Jalili, V., Afgan, E., Gu, Q., Clements, D., Blankenberg, D., Goecks, J., Taylor, J. and Nekrutenko, A. (2020) The Galaxy platform for accessible, reproducible and collaborative biomedical analyses: 2020 update. *Nucleic Acids Res.*, **48**, W395–W402.
  30. Tropberger, P., Pott, S., Keller, C., Kamieniarz-Gdula, K., Caron, M., Richter, F., Li, G., Mittler, G., Liu, E.T., Bühler, M. *et al.* (2013) Regulation of transcription through acetylation of H3K122 on the lateral surface of the histone octamer. *Cell*, **152**, 859–872.
  31. Moon, S.J., Jeong, B.C., Kim, H.J., Lim, J.E., Kim, H.J., Kwon, G.Y., Jackman, J.A. and Kim, J.H. (2021) Bruceantin targets HSP90 to overcome resistance to hormone therapy in castration-resistant prostate cancer. *Theranostics*, **11**, 958–973.
  32. Petrova, T.V., Nykanen, A., Norrmen, C., Ivanov, K.I., Andersson, L.C., Haglund, C., Puolakkainen, P., Wempe, F., von Melchner, H., Gradwohl, G. *et al.* (2008) Transcription factor PROX1 induces colon cancer progression by promoting the transition from benign to highly dysplastic phenotype. *Cancer Cell*, **13**, 407–419.
  33. Schmid, F., Wang, Q., Huska, M.R., Andrade-Navarro, M.A., Lemm, M., Fichtner, I., Dahlmann, M., Kobelt, D., Walther, W., Smith, J. *et al.* (2016) SPON2, a newly identified target gene of MACC1, drives colorectal cancer metastasis in mice and is prognostic for colorectal cancer patient survival. *Oncogene*, **35**, 5942–5952.
  34. Rahnamoun, H., Lu, H., Duttke, S.H., Benner, C., Glass, C.K. and Lauberth, S.M. (2017) Mutant p53 shapes the enhancer landscape of cancer cells in response to chronic immune signaling. *Nat. Commun.*, **8**, 754.
  35. Cho, K.F., Branon, T.C., Udeshi, N.D., Myers, S.A., Carr, S.A. and Ting, A.Y. (2020) Proximity labeling in mammalian cells with TurboID and split-TurboID. *Nat. Protoc.*, **15**, 3971–3999.
  36. Guillemette, B., Drogaris, P., Lin, H.H., Armstrong, H., Hiragami-Hamada, K., Imhof, A., Bonneil, E., Thibault, P., Verreault, A. and Festenstein, R.J. (2011) H3 lysine 4 is acetylated at active gene promoters and is regulated by H3 lysine 4 methylation. *PLoS Genet.*, **7**, e1001354.
  37. Tan, Y., Li, Y. and Tang, F. (2020) Oncogenic seRNA functional activation: a novel mechanism of tumorigenesis. *Mol. Cancer*, **19**, 74.
  38. Kwon, M., Park, K., Hyun, K., Lee, J.H., Zhou, L., Cho, Y.W., Ge, K., Skalnik, D.G., Muir, T.W. and Kim, J. (2020) H2B ubiquitylation enhances H3K4 methylation activities of human KMT2 family complexes. *Nucleic Acids Res.*, **48**, 5442–5456.
  39. Thompson, P.R., Wang, D., Wang, L., Fulco, M., Pediconi, N., Zhang, D., An, W., Ge, Q., Roeder, R.G., Wong, J. *et al.* (2004) Regulation of the p300 HAT domain via a novel activation loop. *Nat. Struct. Mol. Biol.*, **11**, 308–315.
  40. Messier, T.L., Gordon, J.A., Boyd, J.R., Tye, C.E., Browne, G., Stein, J.L., Lian, J.B. and Stein, G.S. (2016) Histone H3 lysine 4 acetylation and methylation dynamics define breast cancer subtypes. *Oncotarget*, **7**, 5094–5109.
  41. Hu, D., Gao, X., Morgan, M.A., Herz, H.M., Smith, E.R. and Shilatifard, A. (2013) The MLL3/MLL4 branches of the COMPASS family function as major histone H3K4 monomethylases at enhancers. *Mol. Cell Biol.*, **33**, 4745–4754.
  42. Cho, Y.W., Hong, T., Hong, S., Guo, H., Yu, H., Kim, D., Guszczynski, T., Dressler, G.R., Copeland, T.D., Kalkum, M. *et al.* (2007) PTIP associates with MLL3- and MLL4-containing histone H3 lysine 4 methyltransferase complex. *J. Biol. Chem.*, **282**, 20395–20406.
  43. Lavery, W.J., Barski, A., Wiley, S., Schorry, E.K. and Lindsley, A.W. (2020) KMT2C/D COMPASS complex-associated diseases [K(CD)COM-ADs]: an emerging class of congenital regulopathies. *Clin. Epigenet.*, **12**, 10.
  44. Tang, Z., Chen, W.Y., Shimada, M., Nguyen, U.T., Kim, J., Sun, X.J., Sengoku, T., McGinty, R.K., Fernandez, J.P., Muir, T.W. *et al.* (2013) SET1 and p300 act synergistically, through coupled histone modifications, in transcriptional activation by p53. *Cell*, **154**, 297–310.
  45. Johnson, G.S., Rajendran, P. and Dashwood, R.H. (2020) CCAR1 and CCAR2 as gene chameleons with antagonistic duality: preclinical, human translational, and mechanistic basis. *Cancer Sci.*, **111**, 3416–3425.